Simulation of Sound Propagating over Soft Surface Using the Equivalent Source Method

Daniel Teye Ocansey

North Carolina A&T State University

A thesis submitted to the graduate faculty

in partial fulfillment of the requirements for the degree of

MASTER OF SCIENCE

Department: Computational Science and Engineering

Major: Computational Science and Engineering

Major Professor: Dr. Marwan Bikdash

Greensboro, North Carolina

2014

The Graduate School
North Carolina Agricultural and Technical State University
This is to certify that the Master's Thesis of

Daniel Teye Ocansey

has met the thesis requirements of
North Carolina Agricultural and Technical State University

Greensboro, North Carolina
2014

Approved by:

Dr. Marwan Bikdash Major Professor & Department Chair	Dr. Kenneth M Flurchick Committee Member
Dr. Dukka KC Committee Member	Dr. Sanjiv Sarin Dean, The Graduate School

Biographical Sketch

Daniel Teye Ocansey was born in January 1, 1987 in Tema, Ghana. He received his Bachelor of Science degree in Mathematics from the Kwame Nkrumah University of Science and Technology in Ghana in the year 2011. He is a candidate for Master's in the Department of Computational Science and Engineering at the North Carolina Agricultural and Technical State University.

Dedication

This work is dedicated to my mother and senior sister.

Acknowledgments

I would thank my mum, Mary Ocansey, for her prayers and for providing me with the motivation to pursue the MSc. degree. I would like to sincerely thank Dr. Marwan Bikdash for his excellent guidance and support without which this thesis would not have been possible. I would like to express my thanks to all of the committee members: Dr. Kenneth M Flurchick and Dr. Dukka KC for the guidance they have provided during my research.

I wish to thank Aiman Albarakati, Hamzeh Qabaja, Mariama Oumarou and all of the members of the Advanced Robotics Laboratory for their advice and encouragement.

Table of Contents

List of Figures

List of Tables

Notations

Variable/ Function	Meaning
ϱ	The flow resistivity
ρ	Density of the air
k	The wavenumber
c	Speed of sound in air
ς	Dummy integration variable for the complex location
Z_0	Ground impedance
μ	The instant time of the Gaussian pulse
σ	The spread of the Gaussian pulse
N_s	Number of sources
N_t	Number of interest points
$H\ and - H$	Main and Image source heights from the surface respectively
$\bar{A}$	The Amplitude of the geometric surface
$\bar{\theta}$	The phase angel of the geometric surface
$\bar{\lambda}$	The wavelength of the geometric surface
$y = \Gamma(x)$	The surface geometry
$\vec{n}(x_i)$	Normal vector at the i^{th} interest point
r_i	Position vector of the i^{th} test point
s_j	Position vector of the j^{th} source
s_H	Position vector of the main source
s_{-H}	Position vector of the image source

A_j	Complex amplitude of the j^{th} equivalent source
R_{Hi}	$\left\|\|s_H - r_i\|\right\|$; Distance from main source $s_H$to the interest point r_i
R_{-Hi}	$\left\|\|s_{-H} - r_i\|\right\|$; Distance from image source $s_{-H}$to the interest point r_i
R_{ji}	$\left\|\|s_j - r_i\|\right\|$; Distance from interest points r_i to the j^{th} equivalent sources s_j
$\hat{R}$	Complex distance between paraxial source at $-H$ and i^{th} test point
$p(r,t)$	The solution at point r and time t
$g(r,t;r',t')$	Free space response at r, t due to a pulse at r' and time t'
$\bar{g}(R,t)$	Form of free-space Green's function in terms of the distance R to the source point
$G(R,k), G(r,S,k)$	Form of free-space harmonic Green's function in terms of the distance R due to sources in set S
$\phi(r,S,k)$	The complex amplitude solution at location r due a source with wavenumber k
$\mathfrak{V}(\mathrm{r},\mathrm{H},\mathrm{k})$	The complex amplitude solution due to paraxial sources
β_i	$\vec{n}(x_i)\cdot\nabla\mathfrak{V}(\mathrm{r},\mathrm{H},\mathrm{k})$ The boundary condition
$\psi(r,S,k)$	$\vec{n}(x_i)\cdot\nabla\phi(r,S,k)$ One harmonic boundary condition
$v(t)$	The step function
$\eta(t;\mu)$	Gaussian pulse centered at $t=\mu$
$q(r,t;\mu)$	Response at r and t to a unit Gaussian pulse $\eta(t;\mu)$

Abstract

Noise generated by large explosions at military bases causes discomfort to residents living in the vicinity, for up to 20km away. This noise explosion has strong low-frequency content and can travel over long distances. Most of the theoretical and experimental work that has been done to study and reduce this type of noise involved the use of barriers and sound proofing the residential houses. In this thesis, we consider the application of reducing the acoustic noise by shaping the landscape. The solution of this problem is difficult due to the semi-infinite domain, especially in the case of soft ground. To overcome the difficulty of calculating a faraway acoustic field for an undulating soft surface, we use the Equivalent Source Method (ESM) as a generalization of the image source method which is applicable to flat surfaces only. Additional sources are used to account for the undulation, and their amplitudes and phases and locations are determined by solving a least-square problem derived from the boundary conditions. The method then estimates the pressure field using superposition of the effect of the equivalent sources. In short, the acoustic field caused by a source above an impedance plane is computed by using a superposition of equivalent point sources located below the surface. A special notation is derived to simplify this formulation.

To account for finite impedance, we incorporate an integral introduced by Ochmann [31] which represents additional sources located at complex locations paraxial to the image source. This integral is known to be convergent for acceptable impedance. The boundary conditions are then updated as to reflect the influence of the Ochamann term, and the matrices involved in the least-squares solution now have six additional terms.

The proposed method is then applied to a sinusoidally varying surface. To simplify the calculation, the positions of the equivalent sources are postulated to be a small distance below the

surface to avoid unnecessary complications due to singularity within the domain. Subsequently the complex amplitudes are derived by enforcing the boundary conditions at a number of test points chosen along the flat and the undulating parts of the surface. The resulting equivalent sources presented inversely decaying amplitudes as expected and their phases presented an expected pattern. Subsequently, we computed the pressure at the far field and both the undulation and the impedance were shown to contribute to the suppression of the acoustic field faraway.

CHAPTER 1

INTRODUCTION

The increase in airplanes, trains and military produces a lot of noise in the environment. These noises are mostly generated by gunfire, explosions, artillery fires, and military vehicles such as airplanes, tanks, and personnel carrier vehicles. Noise generated by large explosions can be heard up to several kilometers away as they move with strong low-frequency content that is not dissipated rapidly in the atmosphere. The rampant nature of low-frequency noise also presents many acoustic problems to architects, designers and planners.

This research focuses on low-frequency outdoor noise and addresses some of the problems associated with modeling it in particular, we look at the difficult problem of simulating acoustic propagation over a hard or soft undulating surface for long distance. We use the equivalent source method (least squares method) algorithm to estimate the acoustic loss over a given ground surface, whether hard or soft.

1.1 Motivation

The noise generated at the military base (e.g. explosions and gunfire, etc.) can be considered as unwanted. This low-frequency noise causes a lot discomfort to resident located miles away. Structures with low resonant frequencies such as windows rattle as a result of their interaction with low-frequency sound (especially when the noise is below the audible range 20Hz). Structures, with a low resonant frequency, such as windows, tables, plates etc. vibrate or rattle as a result of their interaction with low-frequency noise.

In order to gain a better understanding of this phenomenon, we summarize below the characteristics of relevant sources of the noise, propagation characteristics attenuation in the atmosphere, and the interaction between the low-frequency noise and structures.

Reed [36] observed the atmospheric attenuation rate of an explosion wave. He discussed various attenuation factors and the relationships of frequency to the total wave pressure signature of an explosion wave. He concluded that the attenuation is approximately proportional to the five-fourths power of frequency rather than the square of the frequency. The faster attenuation is probably caused by the combination of molecular relaxation with small-scale in homogeneities and turbulence which are usually present in real atmosphere. Lyon [25] reviewed the noise reduction of rectangular enclosure with one flexible wall. He computed the noise reduction for very low frequencies where wall and enclosed volume are stiffness-controlled and for frequencies where the wall is resonant.

West [43] used the ray tube method to predict atmospheric acoustic propagation. A ray tube consists of four rays surrounding a central ray launched from an initial surface close to the source. This method is made of two components. One is the ray path calculation and the other is a prediction of pressure levels along elementary ray tubes from a set of neighboring rays. An invariant property of the ray tube is used to calculate the peak pressure attenuation between a sphere of radius 100m centered to a source and a given ground point. Comparison shows a reasonable agreement between the predictions and measurements obtained in enhancement regions.

Morse [29] considered the transmission of sound through a circular membrane in a plane wall. The setup involves a plane and a rigid wall with circular window across. This stretches the tension between the membrane when it comes in contact with an acoustic medium on both sides. One side of the wall was excited by a plane wave and the solution for transmission through a membrane of finite sizes is obtain. He showed how the resonances and anti-resonances for a finite membrane can modify the transparency effect.

Schomer [38] used the paired-comparison testing method with panels of subjects to determine the acoustical benefits of improved blast noise reduction by retrofitting windows. Two houses were used for this study: One received a retrofit window while the other remained with the older window. C-4 plastic explosives were set off approximately 1.2km away from the houses. Loud speakers were also placed inside each house to produce white noise. They concluded that retrofit windows are highly effective in providing enhanced sound isolation for blast noise. Schomer's data clearly shows that retrofit window provide about 14 dB improvement in terms of annoyance.

Kim and Kim [18] found the sound frequency characteristics to be totally dependent on the properties of the plate. Mostly for a low frequency region where the cavity mode does not occur. They used near field acoustic holography to estimate the sound field variables. They observed pressure to have two types of coupling mechanisms depending on the frequency and wavelength. One mechanism is when the plate and the cavity are strongly coupled. With the plate acting as a source. The second mechanism is when the coupling interaction behavior decreases the radiation efficiency.

Schomer and Averbuch [39] studied the indoor human response to blast sound that generate rattle or vibration. Their objective is to systematically test the subjective response to the presence or absence of rattles in similar blast sound environments and to see if there are structural changes that could reduce annoyance within the indoor blast environment. They did the experiment using a specifically constructed test house and a highly repeatable shake table to simulate the blast sounds. The shake table was used as a giant loudspeaker to generate a blast type waveform and to achieve a peak flat-weighted sound pressure level at the face of the building up to 123dB. To reduce annoyance, the main wall of the house was stiffened. They found that the

stiffening of the main wall does not reduce the resulting blast noise annoyance.

Fawcett [13] used the complex-image method to efficiently approximate the half-space Green's function for acousto-elastic propagation. Fawcett's approximation approach is valid for both the near and far fields. Jeans and Mathews [16] investigated the robustness of the superposition method by using a hybrid of monopole and dipole sources to overcome the problem of non-uniqueness at certain frequencies.

1.2 Abatement Method of the Low-Frequency Noise

Noise impact can vary greatly from a nuisance to adverse effect on a person's health [19]. It is important that we find an effective method to suppress outdoor noise. Over the past several years many have investigated different methods to combat outdoor noise including the use of barriers, screens and replacing residential house windows with noise resistant windows [11, 21, 26, 32, 37].

One popular approach to reduce outdoor low-frequency noise is the use of a barrier. This barrier or wall contains some type of sound-absorbing material. The method of soundproofing the windows and insulating the residential walls become the next option. Bradley and Birta [7] measured the sound transmission loss of exterior wood stud walls and determined that the performance is poor for low frequency sounds. In the past decade, most researchers have theoretically and experimentally worked to reduce the impact of the outdoor low-frequency noise, [6, 7, 22, 32, 41].

The interaction between the low-frequency noise and surface structures is also a major concern. Baker [2] analyzed the pressure profiles of an explosive air blast and discussed methods of computation and the blast experimentation. He provided tables and graphs of compiled blast parameters.

Many have proposed contouring of the landscape or undulating as an anti-propagation method to suppress the low-frequncey wave [41]. The effects of undulating surfaces on propagating acoustic waves have also been studied. Kundu et al. [22] showed that undulating surface can attenuate certain frequencies. To target specific frequencies for elimination, one would have to consider the wavelength and amplitude of the undulating.

Lord Raleigh [35] was the first to theoretically analyze acoustic propagation over undulating surfaces. Other investigations involving rough surfaces were conducted by Potel [34] and Fawcett [12]. Saunders [14] measured the pressure waveform at 1000m from small unconfined charges (e.g. 125-g and 1-kg) of plastic explosive in free air. He concluded that the propagation over concrete and water have similar waveforms while propagation over grass have high frequency content resulting in a different waveform. This paper is very useful for studying underwater explosions.

1.3 Modeling Methods

Highly significant progress in acoustic field modeling have been made using the finite element and the boundary element methods. Bangash [3] provides details with a comprehensive study of the structural dynamic impact of explosion by providing a survey of types of aircraft, missiles, bombs and detonators. In addition, he included empirical models for different materials, water surfaces, soil and rock medium. This book is very useful for studying the interaction between blast sounds and structures.

In the 1990s, Koopmann [20, 40] used these method to model the acoustic field over an unbounded surface. The difficulty of approximating the Helmholtz integral in the numerical form and the singularity of Green's function increases the computational complexity. Koopmann investigated the principle of wave superposition to compute acoustic field. This method offers

several advantages over the boundary-element method including a decrease in computational complexity and it improves the accuracy for a similar density calculations.

Due to its computational cost especially in a semi-finite domain, our purpose is to propose an alternative method to model the effects of surfaces on outdoor acoustic waves using equivalent sources (hard surfaces) or complex equivalent sources (soft surfaces).

Bikdash and Meng [42] modeled a hard and undulating surface shape (e.g. flat surface, hill, valley etc.) using the equivalent source method. They placed the equivalent sources at various distances below the surface. Johnson [17] used the equivalent source method to compute the internal pressure field for an enclosure with arbitrary boundary condition and internal objects scattering the sound wave. A rectangular box with rigid wall is used as the enclosure. The approximation of the behavior of the boundary is determined by the strength of the equivalent sources. The source strengths must be calculated before the pressure field can be approximated. This method have been further studied by Nelson and Yoon [27, 28].

Pinho and Arruda [33] compared the equivalent source method with NAH and concluded that good acoustic source reconstruction can be obtained using the ESM. Bouchet [5] used an equivalent sphere of the equivalent sources where each point on the structure corresponds to a point on the sphere. This method is further studied on sound propagation through a street canyon by Forssen [15].

Attenborough [1] measured and modeled the ground effect arising from the interaction between sound traveling directly from source to receiver and sound the reflected from the ground are emphasized. He focused on the ground porosity, the layering style, the small-scale surface roughness and with tall vegetation. Brick and Ochmann [4] computed the corresponding Green's function which describes the sound propagation above an impedance plane and implemented it

using the Boundary Element Method (BEM). This is based on the superposition of sound sources with complex source locations. The evaluation of Green's function includes the sound radiation from burning flames above ground and tire-road noise. Wu and Seybert [23] used the boundary element method (BEM) to model acoustic radiation and scattering from bodies of arbitrary shape in close proximity of an infinite plane. They also attempted to derive the Green's function for negative reactance boundary conditions, but many difficulty proved insurmountable.

Ochmann [30] developed a simulation technique to replace the radiating body by a system of simple sources located within the envelope of the radiator. This simulated field reproduces the original field depending on the amplitude and the boundary conditions. Li and White [24] introduced an efficient method for computing the sound field near the region above an impedance ground or an extended reaction ground. Their procedure is based on complex image theory. The result can be exactly tested using the Sommerfeld identity.

Ochmann [31] calculated the sound pressure field caused by a monopole source above an impedance plane using the superposition of the equivalent sources located along a line in the mirror space. The main idea is to use the superposition of equivalent sources but to allow these sources to have complex location. This approach is called the complex equivalent source method (CESM). This method is suitable for both masslike and springlike surface impedances and can be use in place of the boundary element method. These methods have been investigated by many researchers [6].

1.4 Synopsis

In Chapter 2, we discuss the acoustic waves and its boundary conditions. In Chapter 3, we discuss the response due to a single harmonic and its boundary conditions. Chapter 4 introduces the equivalent source method (ESM) and describes the utilization of ESM to model the acoustic

loss over a rigid undulating ground surface, and calculates the least-square solution. In Chapter 5, we introduce the complex equivalent source method (CESM) to model the acoustic loss over a soft surface. The least squares method is used to estimate the complex amplitude (strength) of these equivalent sources. The simulations for this thesis were done using Matlab and Mathematica.

CHAPTER 2

THEORETICAL BACKGROUND

This chapter reviews the theory of sound waves. The propagation of waves can be described as a hyperbolic partial differential equation knwon as the wave equation. Section 2.1 discusses the wave equation. The various boundary conditions are discussed in Section 2.2. The wave equation in an unbounded homogenous and time invariant medium leads to Green's function. This is discussed in Section 2.3. The response to a harmonic and a Gaussian pulse is discussed in Sections 2.4 and 2.5 respectively.

2.1 The Wave Equation in Unbounded Space

The wave equation is derived using the equation of state, continuity equation and Newton's equation of motion. The equation is given as

$$c^2 \nabla^2 p\left(r,t\right) - \frac{\partial^2}{\partial t^2} p\left(r,t\right) = f\left(r,t\right) \tag{2. 1}$$

where the Laplacian operator ∇ expresses the spherical coordinates, $p\left(r,t\right)$ is the pressure field (velocity potential) at point $r \in \mathbb{R}^3$, time t, c is the speed of sound and $f\left(r,t\right)$ is distributed source excitation at point r and time t.

If $f\left(r,t\right)$ is bounded and is nonzero only in a bounded domain $\Gamma \subset \mathbb{R}^3$ then the pressure $p\left(r,t\right)$ is expected to decay to zero away from Γ according to the Sommerfield conditions:

$$\lim_{r\to\infty} p = O\left(r^{-1}\right) \tag{2. 2}$$

$$\lim_{r\to\infty} \left(\frac{\partial}{\partial r} - \frac{1}{c}\frac{\partial}{\partial t}\right) p = o\left(r^{-1}\right) \tag{2. 3}$$

In general, the right hand side of Equation (2.2) or (2.3) is expressed as

$$\lim_{r\to\infty} p = O\left(r^{(n-1)/2}\right) \quad (2.4)$$

$$\lim_{r\to\infty}\left(\frac{\partial}{\partial r}-\frac{1}{c}\frac{\partial}{\partial t}\right)p = o\left(r^{(n-1)/2}\right), \quad (2.5)$$

where n represents the dimensions in space. For $n = 2$ (two dimensional space) the pressure is

$$O\left(r^{1/2}\right). \quad (2.6)$$

2.2 The Wave Equation over a Surface

When acoustic waves propagate over an outdoor surface Γ, the sound pressure $p(r,t)$ must satisfy the additional boundary condition in Equation (2.8):

$$c^2\nabla^2 p(r,t) - \frac{\partial^2}{\partial t^2}p(r,t) = f(r,t) \quad (2.7)$$

$$\frac{\partial p(r,t)}{\partial \overrightarrow{n}} + \frac{1}{Z_0 c}\frac{\partial p(r,t)}{\partial t} = 0 \quad (2.8)$$

$$\lim_{r\to\infty} p = O\left(r^{-1}\right) \quad (2.9)$$

$$\lim_{r\to\infty}\left(\frac{\partial}{\partial r}-\frac{1}{c}\frac{\partial}{\partial t}\right)p = o\left(r^{-1}\right) \quad (2.10)$$

where Z_0 is the ground impedance and $\overrightarrow{n}$ being the unit vector that is orthogonal to the boundary surface. If the ground surface is assumed to be a hard surface then the ground impedance Z_0 is infinite and hence Equation (2.8) is expressed

$$\overrightarrow{n}\cdot\nabla p(r,t) = 0 \quad (2.11)$$

For a soft ground surface, Equation (2.8) can be written as

$$\overrightarrow{n}\cdot\nabla p(r,t) = -\frac{1}{Z_0 c}\frac{\partial p(r,t)}{\partial t},$$

where ∇ is the gradient vector in Cartesian coordinates.

2.3 Green's Functions for Unbounded Space

The unbounded-space Green's function is the solution of Equation (2.1)-(2.3) and it represents the response pressure $p(r,t)$ due to a unit pulse applied at r' and t':

$$f(r,t) = \delta(r-r')\,\delta(t-t'),\ \ f:\mathbb{R}^3\times\mathbb{R}\to\mathbb{R} \tag{2.12}$$

The unbounded-space Green's function denoted by $g(r,t;r',t')$ must satisfy

$$g(r,t;r',t') = 0,\ t\le t', \tag{2.13}$$

$$\frac{\partial}{\partial t}g(r,t;r',t') = 0,\ t\le t', \tag{2.14}$$

and must also satisfy the causality condition. In particular, Equation (2.1) becomes

$$\left(\frac{\partial^2}{\partial t^2} - c^2\nabla^2\right) g(r,t;r',t') = \delta(r-r')\,\delta(t-t') \tag{2.15}$$

Theorem: *Green's function $g(r,t;r',t')$ which is the pressure at the time t and position r due to an impulse at the point r' at time t' in unbounded homogenous time-invariant space is given by*

$$g(r,t;r',t') = \frac{\delta(t-t'-||r-r'||/c)}{4\pi c^2||r-r'||},\ \ g:\mathbb{R}^3\times\mathbb{R}\times\mathbb{R}^3\times\mathbb{R}\to\mathbb{R}. \tag{2.16}$$

If the space is homogenous and time invariant then $g(r,t,r';t')$ is equal in value to

$$\bar{g}(r-r',t-t') = \frac{\delta(t-t'-||r-r'||/c)}{4\pi c^2||r-r'||},\ \ g:\mathbb{R}^3\times\mathbb{R}\to\mathbb{R} \tag{2.17}$$

and $R = ||r-r'||$, then one can write Equation (2.16) as

$$\bar{g}_1(R,t-t') = \frac{\delta(t-t'-R/c)}{4\pi c^2 R},\ \ \bar{g}_1:\mathbb{R}^2\times\mathbb{R}\to\mathbb{R} \tag{2.18}$$

Proof: The unbounded homogenous and time invariant Green's function $g(r,t;r',t')$

satisfies

$$\left(\frac{\partial^2}{\partial t^2} - c^2\nabla^2\right) g\left(r,t;r',t'\right) = \delta\left(r-r'\right)\delta\left(t-t'\right), \tag{2. 19}$$

If the Laplace transform is

$$\hat{f}\left(\bar{s}\right) = \mathcal{L}_{t\to\bar{s}}\left\{f\left(t\right)\right\} = \int_0^\infty e^{-\bar{s}t} f\left(t\right) dt, \tag{2. 20}$$

then

$$\hat{g}\left(r,\bar{s};r',t'\right) = \mathcal{L}_{t\to\bar{s}}\left\{g\left(r,t;r',t'\right)\right\} = \int_0^\infty e^{-\bar{s}t} g\left(r,t;r',t'\right) dt. \tag{2. 21}$$

Taking the Laplace transform of the left hand side (LHS) of Equation (2.19) yields

$$\begin{aligned}
\mathcal{L}_{t\to\bar{s}}\left\{\frac{\partial^2 g}{\partial t^2} - c^2\nabla_r^2 g\right\} &= \bar{s}^2\mathcal{L}_{t\to\bar{s}}\left\{g\right\} - g|_{t=0} - \frac{\partial g}{\partial t}|_{t=0} - c^2\mathcal{L}_{t\to\bar{s}}\left\{\nabla^2 g\right\} \qquad (2.\ 22)\\
&= \bar{s}^2\mathcal{L}_{t\to\bar{s}}\left\{g\right\} - c^2\nabla^2\mathcal{L}_{t\to\bar{s}}\left\{g\right\}\\
&= \bar{s}^2\hat{g} - c^2\nabla^2\hat{g},
\end{aligned}$$

where the boundary conditions in Equations (2.13) and (2.14) were used to drop the two terms above. The Laplace of the RHS of Equation (2.19) gives

$$\begin{aligned}
\mathcal{L}_{t\to\bar{s}}\left\{\delta\left(r-r'\right)\delta\left(t-t'\right)\right\} &= \int_0^\infty e^{-\bar{s}t}\delta\left(t-t'\right)\delta\left(r-r'\right) dt \qquad (2.\ 23)\\
&= e^{-\bar{s}t'}\delta\left(r-r'\right)
\end{aligned}$$

Equating both sides of Equation (2.22) and (2.23) yields

$$\left(\bar{s}^2\hat{g} - c^2\nabla^2\hat{g}\right) = e^{-\bar{s}t'}\delta\left(r-r'\right). \tag{2. 24}$$

In spherical coordinates, the operator $\nabla^2\hat{g}$ can be written as

$$\nabla^2\hat{g} = \frac{1}{R^2}\frac{\partial}{\partial R}\left(R^2\frac{\partial\hat{g}}{\partial R}\right) + \frac{1}{R^2\sin\theta}\frac{\partial}{\partial\theta}\left(\sin\theta\frac{\partial\hat{g}}{\partial\theta}\right) + \frac{1}{R^2\sin^2\theta}\frac{\partial}{\partial\theta}\frac{\partial\hat{g}}{\partial\bar{\theta}}, \tag{2. 25}$$

where $\bar{\theta}$ and θ represent the Azimuthal angle and Zenith angle or co-latitude. However one can assume that the derivatives of $\hat{g}\left(r,\bar{s};r',t'\right)$ with respect to θ and $\bar{\theta}$ will vanish. Therefore,

$$\begin{aligned}\nabla^2\hat{g} &= \frac{1}{R^2}\frac{\partial}{\partial R}\left(R^2\frac{\partial\hat{g}}{\partial R}\right)=\frac{1}{R^2}\left(2R\frac{\partial\hat{g}}{\partial R}+R^2\frac{\partial^2\hat{g}}{\partial R^2}\right) \quad (2.\ 26)\\ &= \frac{2}{R}\frac{\partial\hat{g}}{\partial R}+\frac{\partial^2\hat{g}}{\partial R^2}\end{aligned}$$

which is valid if the medium is unbounded homogenous and time invariant and $r-r'$ is the radial vector measured from the source location r' as the origin. Substituting Equation (2.26) into Equation (2.24) yields

$$\bar{s}^2\hat{g}-c^2\left(\frac{2}{R}\frac{\partial\hat{g}}{\partial R}+\frac{\partial^2\hat{g}}{\partial R^2}\right)=e^{-\bar{s}t'}\delta\left(R\right). \quad (2.\ 27)$$

The homogeneous solution of Equation (2.27)

$$\bar{s}^2\hat{g}-\frac{2c^2}{R}\frac{\partial\hat{g}}{\partial R}-c^2\frac{\partial^2\hat{g}}{\partial R^2}=0, \quad (2.\ 28)$$

is given as

$$\hat{g}\left(r,\bar{s};r',t'\right)=\hat{A}\frac{e^{-\frac{R\bar{s}}{c}}}{R}, \quad (2.\ 29)$$

which can be verified by directly substituting $\hat{g}\left(r,\bar{s};r',t'\right)$ into Equation (2.27). To find the constant $\hat{A}$, we integrate Equation (2.27) over a small volume V_m of a ball B_m centered at $R=0$ (i.e. at r') and of radius m:

$$\begin{aligned}I_1 &= \int_{B_m}\left(\bar{s}^2\hat{g}-c^2\nabla^2\hat{g}\right)dV=\int_V e^{-\bar{s}t'}\delta\left(R\right)dV \quad (2.\ 30)\\ &= e^{-\bar{s}t'} \quad (2.\ 31)\end{aligned}$$

The limit as $m\to 0$ of the LHS of Equation (2.30)

$$\lim_{m\to 0}\int_{B_m}\left(\bar{s}^2\hat{g}\right)dV-\lim_{m\to 0}\int_{B_m}\left(c^2\nabla^2\hat{g}\right)dV, \quad (2.\ 32)$$

can be simplified as $\lim_{m\to 0}\int_{B_m}(\bar{s}^2\hat{g})\,dV = 0$ because $\hat{g} = O\left(\frac{1}{R}\right)$ and by noting that $dV = O(R^3)$. The second term is computed using the using the divergence theorem

$$\int_V \nabla^2\hat{g}dV = \int_S \nabla\hat{g}.\overrightarrow{n}\,dS, \tag{2. 33}$$

which makes the second term of Equation (2.32) to be expressed as

$$I_1 = -\lim_{m\to 0} c^2\int_{B_m}\nabla^2\hat{g}dV = -\lim_{m\to 0} c^2\int_S \nabla\hat{g}.\overrightarrow{n}\,dS \tag{2. 34}$$

with $\nabla\hat{g}$ expressed as

$$\nabla\hat{g} = \frac{\partial}{\partial R}\left(\hat{A}\frac{e^{-\frac{R\bar{s}}{c}}}{R}\right) = \frac{\hat{A}e^{-\frac{R\bar{s}}{c}}\left(-\frac{R\bar{s}}{c}-1\right)}{R^2} \tag{2. 35}$$

Substituting $\nabla\hat{g}$ into Equation (2.34) yields

$$\begin{aligned} I_1 &= \lim_{m\to 0} c^2\int_S \frac{\hat{A}e^{-\frac{R\bar{s}}{c}}\left(\frac{R\bar{s}}{c}+1\right)}{R^2}dS \\ &= \lim_{m\to 0}\frac{\hat{A}\left\{e^{-\frac{m\bar{s}}{c}}\left(\frac{m\bar{s}}{c}+1\right)\right\}}{m^2}c^2 4\pi m^2 = \hat{A}4\pi c^2. \end{aligned} \tag{2. 36}$$

But $I_1 = e^{-\bar{s}t'}$ from Equation (2.30), hence

$$\hat{A} = \frac{e^{-\bar{s}t'}}{4\pi c^2}. \tag{2. 37}$$

Equation (2.29) becomes

$$\hat{g}(r,\bar{s};r',t') = \frac{e^{-\bar{s}t'}}{4\pi c^2}\frac{e^{-\frac{R\bar{s}}{c}}}{R} = \frac{e^{-\bar{s}\left(\frac{R}{c}+t'\right)}}{4\pi c^2 R},$$

Take the inverse Laplace transform of $\hat{g}(r,\bar{s};r',t')$ to obtain:

$$g(r,t;r',t') = \mathcal{L}^{-1}_{\bar{s}\to t}\left\{\hat{g}(r,\bar{s};r',t')\right\} \tag{2. 38}$$

and therefore the free space Green's function for the wave equation is given as:

$$g\left(r,t;r',t'\right)=\frac{\delta\left(t-t'-R/c\right)}{4\pi c^{2}R}=\bar{g}\left(R,t;t'\right) \tag{2. 39}$$

2.4 Response to a Harmonic in Unbounded Space

The response $p\left(r,t\right)$ due to a forcing $f\left(r,t\right)$ is given as the superposition of the Green's function $g(r,t;r',t')$ and the forcing $f\left(r,t\right)$ over the domain Γ as shown in Figure (1) is expressed as

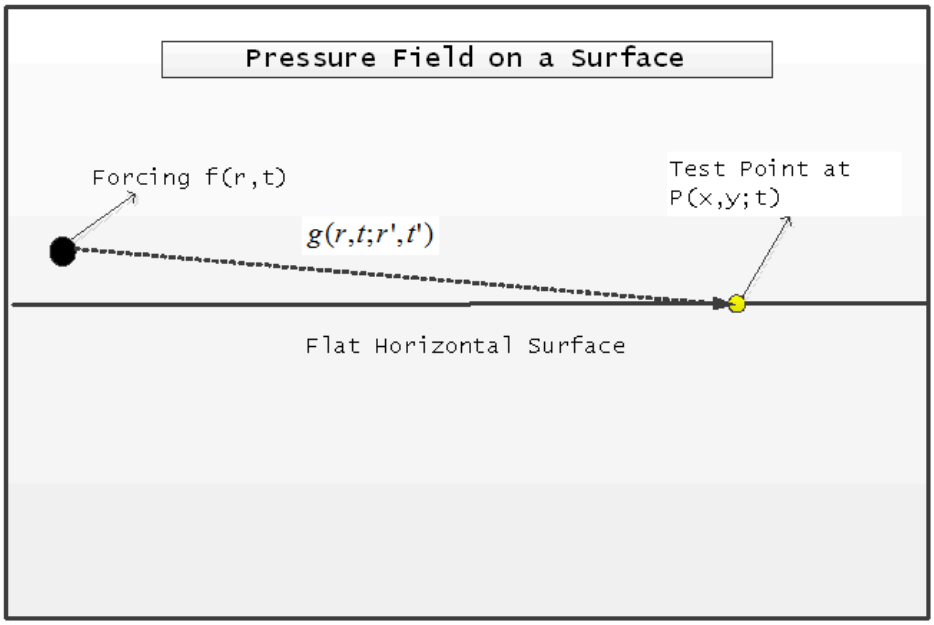

Figure 1. The response due to a source $f(r,t)$

$$p\left(r,t\right)=\iint_{\Gamma}g(r,t;r',t')f\left(r',t'\right)dr'dt', \tag{2. 40}$$

because of the unbounded homogenous and time invariant, Equation (2.40) can also be written as

$$p\left(r,t\right)=\int_{0}^{\infty}g\left(r-r',t-t'\right)f\left(r',t'\right)dt'. \tag{2. 41}$$

Theorem: *The response $p(r,t)$ due a harmonic forcing source*

$$f(r,t) = \delta(r - r')\, e^{\mathbf{j}\omega t} \tag{2. 42}$$

is given as

$$\begin{aligned} p(r,t) &= \frac{e^{-\mathbf{j}kR}}{4\pi c^2 R} e^{\mathbf{j}\omega t} && (2.\ 43)\\ \omega &= 2\pi f && (2.\ 44) \end{aligned}$$

where ω is the angular velocity and f is the frequency.

Proof: The convolution integral in Equation (2.40) is

$$\begin{aligned} p(r,t) &= \int_0^\infty \int_\Gamma g(r,t;r',t')\, f(r',t')\, dr'dt' && (2.\ 45)\\ &= \int_0^\infty \int_\Gamma \frac{\delta(t - t' - ||r - r'||/c)}{4\pi c^2 ||r - r'||} \delta(r - r')\, e^{\mathbf{j}\omega t'} dr'dt'. && (2.\ 46) \end{aligned}$$

The arguments of the δ functions are zero when

$$r = r' \text{ and } t' = t - ||r - r'||/c, \tag{2. 47}$$

and therefore

$$\begin{aligned} p(r,t) &= \frac{\exp\left(\mathbf{j}\omega t - \mathbf{j}\frac{\omega}{c}||r - r'||\right)}{4\pi c^2 ||r - r'||} && (2.\ 48)\\ &= \frac{e^{-\mathbf{j}kR}}{4\pi c^2 R} e^{\mathbf{j}\omega t}. && (2.\ 49) \end{aligned}$$

■

2.5 Response to a Gaussian Pulse in Unbounded Space

Definition: *The unit Gaussian pulse $\eta(t;\mu)$ centered at μ and a spread of σ is given as*

$$\eta(t;\mu) = -(t - \mu)\frac{\exp\left(-(t - \mu)^2/4\sigma^2\right)}{2\sigma^2}. \tag{2. 50}$$

Theorem: *The response* $p\left(r,t\right)$ *due to the unit Gaussian pulse*

$$f\left(r,t\right)=\delta\left(r-r'\right)\eta\left(t;\mu\right)v\left(t\right)$$

is given by

$$p\left(r,t\right)=-\frac{\left(t-\mu-R/c\right)}{8\pi c^{2}\sigma^{2}R}\exp\left(-\left(t-\mu-R/c\right)^{2}/4\sigma^{2}\right)v\left(t-R/c\right) \tag{2. 51}$$

where the function $v\left(t-R/c\right)$ is define as a step function. Figure (2) shows a unit Gaussian pulse $\eta\left(t;\mu\right)$ centered at $\mu=0.5$ second, $\sigma=0.1$, over the duration 0 to 1 second.

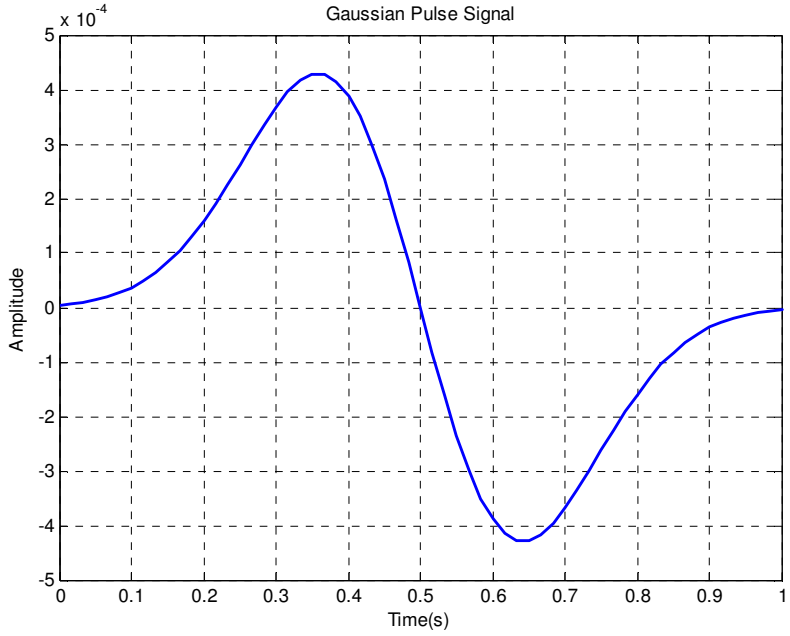

Figure 2. Unit Gaussian pulse $\eta(t;\mu)$ at position r'

Proof: The response $p\left(r,t\right)$ due a pulse $f\left(r,t\right)$ is expressed as

$$p\left(r,t\right) = \int_{0}^{\infty}\int_{\Omega}g\left(r,t;r',t'\right)f\left(r',t'\right)dr'dt' \tag{2. 52}$$

$$= \int_{0}^{\infty}\int_{\Omega}\frac{\delta\left(t-t'-||r-r'||/c\right)}{4\pi c^{2}||r-r'||}\delta\left(r-r'\right)\eta\left(t';\mu\right)v\left(t'\right)dr'dt'. \tag{2. 53}$$

The arguments of the δ functions are zero when

$$r = r' \text{ and } t' = t - ||r - r'|| / c, \tag{2. 54}$$

and therefore,

$$\begin{aligned} p(r,t) &= \frac{\eta(t - ||r - r'|| / c)}{4\pi c^2 ||r - r'||} v(t - ||r - r'|| / c) && (2.\ 55) \\ &= -\frac{(t - \mu - R/c)}{8\pi c^2 R\sigma^2} \exp\left(-(t - \mu - R/c)^2 / 4\sigma^2\right) v(t - R/c). && (2.\ 56) \end{aligned}$$

The function $q(r,t;\mu)$ will be used in place of $p(r,t)$ throughout the thesis. To enforce causality, we expressed $q(r,t;\mu)$ as follows

$$q(r,t;\mu) = \begin{cases} 0 \text{ for } t \leq 0 \\ \frac{1}{4\pi c^2}\eta\left(t - \frac{R}{c};\mu\right) \\ 0 \text{ for } t \geq \frac{R}{c} \end{cases}.$$

■

CHAPTER 3

HARMONIC WAVE PROPAGATION

The physics of wave propagation is explained using some special wave solutions. A harmonize plane wave propagating in a homogeneous medium is examined by simplifying the wave equation as a time independent equation by assuming time-harmonic dependence. This leads to the Helmholtz equation.

3.1 Helmholtz Equation and Boundary Value Problems

The solution to the wave equation in Equations (2.1)-(2.3) for a harmonic source has the form

$$p(r,t) = \phi(r)\, e^{\mathbf{j}\omega t} \tag{3. 1}$$

where $\phi : \mathbb{R}^3 \rightarrow \mathbb{R}$ is a spatial function defined on three-dimensional Euclidean space, ω is the angular frequency and t is time. Substituting Equation (3.1) into Equation (2.1) yields

$$\begin{aligned} c^2\nabla^2\phi(r)\, e^{\mathbf{j}\omega t} - \frac{\partial^2}{\partial t^2}\phi(r)\, e^{\mathbf{j}\omega t} &= f(r,t) \\ c^2\nabla^2\phi(r)\, e^{\mathbf{j}\omega t} + e^{\mathbf{j}\omega t}\phi(r)\,\omega^2 &= f(r,t) \\ \nabla^2\phi(r) + \phi(r)\,\frac{\omega^2}{c^2} &= c^{-2}e^{-\mathbf{j}\omega t} f(r,t), \end{aligned} \tag{3. 2}$$

If $k = \omega/c$, then Equation (3.2) expresses the Helmholtz equation in the form

$$\nabla^2\phi(r) + k^2\phi(r) = c^{-2}e^{-\mathbf{j}\omega t} f(r,t) \tag{3. 3}$$

where k is the wavenumber. Let

$$F(r,k,t) = c^{-2}e^{-\mathbf{j}\omega t} f(r,t). \tag{3. 4}$$

Theorem: *The response $G(r,r',k)$ due to the harmonic source $f(r,t) = c^2 e^{\mathbf{j}\omega t}\delta(r-r')$*

at r' is

$$G\left(r, r', k\right) = \frac{e^{\mathbf{j}kR}}{4\pi R} \tag{3. 5}$$

Proof: The pressure field generated by a point source can be described by the inhomogeneous Helmholtz equation of the form

$$\nabla^2 G\left(r, r', k\right) + k^2 G\left(r, r', k\right) = \delta\left(r - r'\right). \tag{3. 6}$$

If the solution for harmonic source $f\left(r, t\right)$ in Equation (2.42) is given by

$$p\left(r, t\right) = \frac{e^{-\mathbf{j}kR}}{4\pi c^2 R} e^{\mathbf{j}\omega t},$$

then solution for the harmonic source $f\left(r, t\right) = c^2 e^{\mathbf{j}\omega t}\delta\left(r - r'\right)$ in Equation (3.4) is the free field Green's function $G\left(r, r', k\right)$:

$$G\left(r, r', k\right) = \frac{e^{\mathbf{j}kR}}{4\pi R}. \tag{3. 7}$$

■

Green's function $G\left(r, r', k\right)$ is used to compute the pressure field. A single acoustic source in free space is the total complex amplitude of pressure emanates from the point source at r' in unbounded homogenous space

$$\bar{G}\left(R, k\right) = \frac{e^{\mathbf{j}kR}}{4\pi R}. \tag{3. 8}$$

3.2 Harmonic Solution over a Surface

The harmonic pressure propagating above a geometric surface must satisfy.

$$\nabla^2\phi(r) + k^2\phi(r) = c^{-2}e^{-\mathbf{j}\omega t}f(r,t) = F(r,k,t), \tag{3. 9}$$

$$\frac{\partial\phi(r)}{\partial\overrightarrow{n}} + \frac{\mathbf{j}k}{Z_0}\phi(r) = 0, \tag{3. 10}$$

$$\lim_{r\to\infty}\phi = O\left(r^{(1-n)/2}\right), \tag{3. 11}$$

$$\lim_{r\to\infty}\left(\partial_r\phi - \mathbf{j}k\phi\right) = o\left(r^{(1-n)/2}\right), \tag{3. 12}$$

where $\partial/\partial n$ is the derivative in the direction of the normal $\overrightarrow{n}$ and n is the dimension in space. Equations (3.11) and (3.12) define the Sommerfield radiation conditions and Equation (3.10) is the ground boundary condition on the surface. For a soft ground surface Equation (3.10) is expressed as

$$\overrightarrow{n}\cdot\nabla\phi(r) = -\frac{\mathbf{j}k}{Z_0}\phi(r). \tag{3. 13}$$

If the surface of the ground is assumed to be hard then Equation (3.10) becomes

$$\overrightarrow{n}\cdot\nabla\phi(r) = 0. \tag{3. 14}$$

Figure (3) and (4) shows the boundary conditions for the hard and soft geometric surface

3.3 The Ground Impedance

The normalized acoustical impedance Z_0 was computed using the local reaction model. This model is characterized by the complex parameter (e.g. many different kinds of ground such as grassy, hard, sandy ground and other) of the impedance Z_0 . Delancy and Bazley [9] empirically expressed the normal acoustical impedance Z_0 as a function of frequency.

$$\frac{Z_0}{\rho_0 c_0} = 1.0 + 9.08\left(\frac{2\pi\varrho}{\omega}\right)^{0.75} - 11.9\mathbf{j}\left(\frac{2\pi\varrho}{\omega}\right)^{0.73} \tag{3. 15}$$

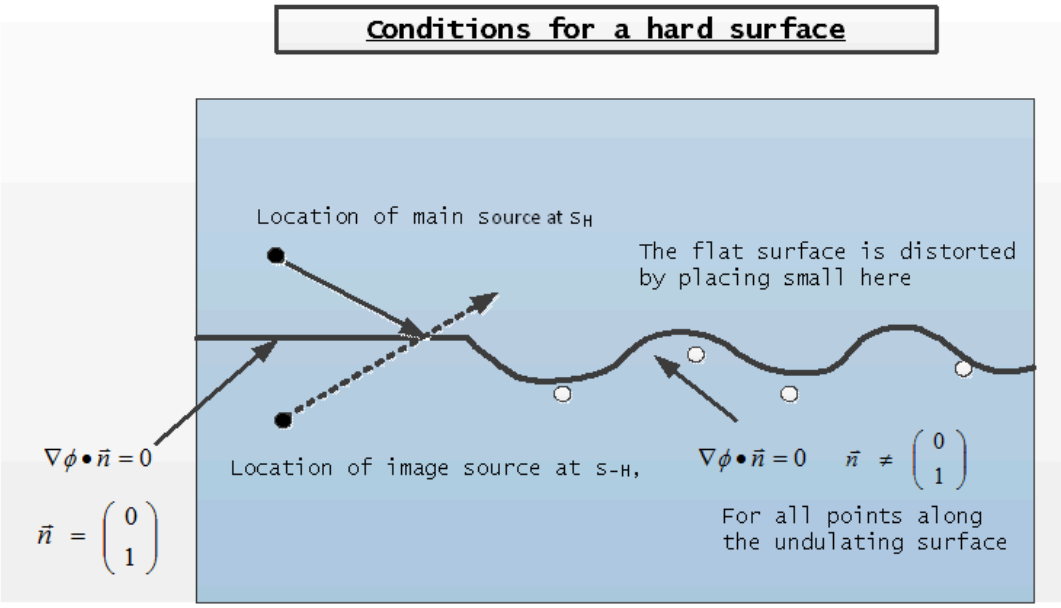

Figure 3. Conditions for hard ground surface

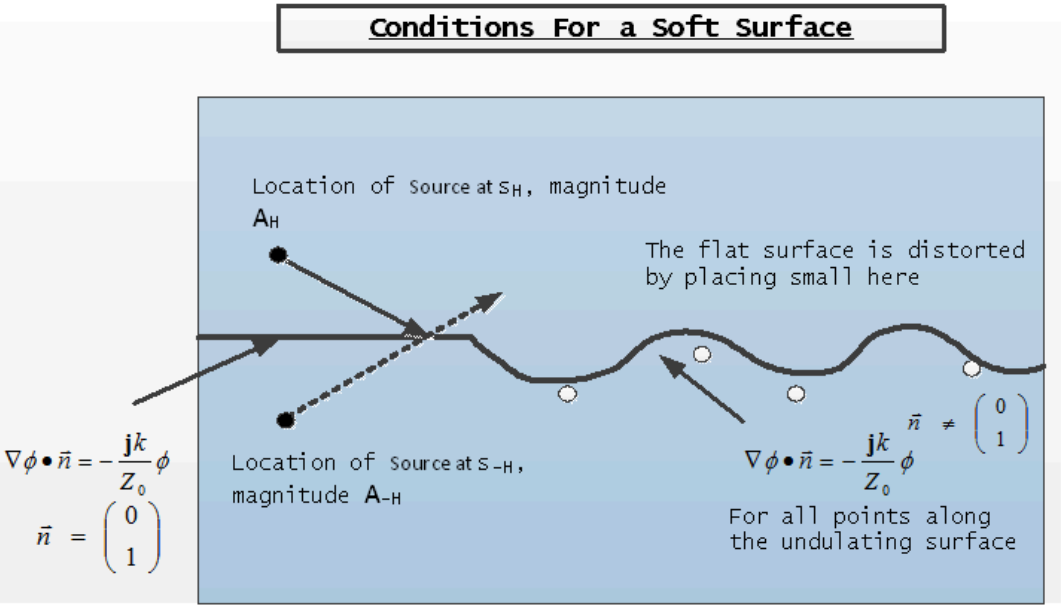

Figure 4. Conditions for soft ground surface

where ϱ is the flow-resistivity measured in cgs units, ρ_0 is the density, c_0 is the velocity of sound, and $\rho_0 c_0$ defines the characteristic impedance of air. Embleton [10] measured the flow-resistivity for different absorbing materials. Table (1) shows the flow-resistivity for different sets of materials.

Table 1. Ranges of effective flow resistivity for various types of ground surface

Description of surface	Flow resistivity cgs rayls (1 cgs rayls = 1000 Pa s/m^2)
Dry snow, new fallen $0.1m$ over about $0.4m$ older snow.	$10 - 30$
Sugar snow	$25 - 50$
In forest, pine, or hemlock.	$20 - 80$
Grass: rough pasture, airport, public buildings, etc.	$150 - 300$
Roadside dirt, ill-defined, small rocks up to $0.1m$ mesh.	$300 - 800$
Sandy silt, hard packed by vehicles.	$800 - 2500$
"Clean" limestone chips, thick layer (0.01 to $0.025m$ mesh.	$1500 - 4000$
Old dirt roadway, fine stone ($0.05m$ mesh) interstices filled.	$2000 - 4000$
Earth, exposed and rain-packed.	$4000 - 8000$
Quarry dust, fine, very hard-packed by vehicles.	$5000 - 20000$
Asphalt, sealed by dust and light use.	~30000
Upper limit set by thermal-conduction and viscous boundary layer	2×10^5 to 1×10^6

CHAPTER 4

HARMONIC MODELING OVER A HARD SURFACE USING EQUIVALENT SOURCES

Modeling the pressure field formed by a radiator of a certain shape using equivalent sources comes with the challenges of determining the strengths of the equivalent sources. Another challenge is determining the placement and the number of sources needed to minimize the field error.

The amplitudes of the equivalent sources are estimated using the least squares method. This method have been used by many researchers in order to minimize the sum of square errors made in solving the exterior and interior acoustic pressure fields [44, 45]. The strengths of the equivalent sources are computed using the same approach. The following sections will give us a detail derivation.

4.1 Description of the Surface Geometry

The geometry $y = \Gamma(x)$ is first specified. The vector normal at the interest point on the surface is determined as follows. The direction of the tangent line (slope) is the only information needed to determine the unit normal vector. If the geometric surface coordinates is given by

$$\overrightarrow{v} \Leftrightarrow (x, \Gamma(x)) = [x, y]^T, \tag{4. 1}$$

then one can compute the unit normal vector $\overrightarrow{n}$ along the surface. The gradient on the y-axis is

$$dy = \Gamma'(x)\, dx \tag{4. 2}$$

$$dl = \sqrt{dx^2 + dy^2} = dx\sqrt{1 + \Gamma'(x)^2} \tag{4. 3}$$

and the unit tangent relation vector $\overrightarrow{t}$ and the unit normal vector $\overrightarrow{n}$ along a surface is expressed

as

$$\overrightarrow{t} \Leftrightarrow \frac{1}{dl}\left[dx, dy\right]^T \quad \text{and} \quad \overrightarrow{n} \Leftrightarrow \frac{1}{dl}\left[-dy, dx\right]^T. \tag{4. 4}$$

For a flat horizontal surface the unit tangent vector $\overrightarrow{t}$ and the unit normal vector $\overrightarrow{n}$ is

$$\overrightarrow{t} \Leftrightarrow \left[\begin{array}{cc} 1 & 0 \end{array}\right]^T \quad \text{and} \quad \overrightarrow{n} \Leftrightarrow \left[\begin{array}{cc} 0 & 1 \end{array}\right]^T. \tag{4. 5}$$

At a point of interest r_i on the surface, the outward unit normal vector $\overrightarrow{n}$ is expressed as

$$\overrightarrow{n}\left(r_i\right) \Leftrightarrow \frac{1}{dl}\left[-\Gamma'\left(x_i\right)dx, dx\right]^T = \frac{1}{\sqrt{1+\Gamma'\left(x_i\right)^2}}\left[-\Gamma'\left(x_i\right), 1\right]^T, \tag{4. 6}$$

with

$$\overrightarrow{n}\left(r_i\right) \Leftrightarrow \left[\begin{array}{c} \cos\nu_i \\ \sin\nu_i \end{array}\right] = \frac{1}{\sqrt{1+\Gamma'\left(x_i\right)^2}}. \left[\begin{array}{c} -\Gamma'\left(x\right) \\ 1 \end{array}\right] \tag{4. 7}$$

and

$$\cos\nu_i \;=\; -\frac{\Gamma'\left(x_i\right)}{\sqrt{1+\Gamma'\left(x_i\right)^2}} \;\text{ and }\; \sin\nu_i = \frac{1}{\sqrt{1+\Gamma'\left(x_i\right)^2}}, \tag{4. 8}$$

where r_i is the i^{th} interest point. An example geometry of the undulating surface is shown in Figure (5) which defines the cross-section of the sinusoidal surface described as

$$y = \Gamma\left(x\right) = \bar{A}\sin\left(\frac{2\pi x}{\bar{\lambda}} + \bar{\theta}\right) \tag{4. 9}$$

where $\bar{A}$ is the amplitude, $\bar{\lambda}$ is the wavelength and $\bar{\theta}$ is the phase angel.

The amplitude, length and phase of the undulating can be changed from one model to another to see what effect these parameters have on the acoustic loss. Figure (6) shows the position of the interest points along the surface, and Figure (7) displays the unit normal vectors at the defined interest points.

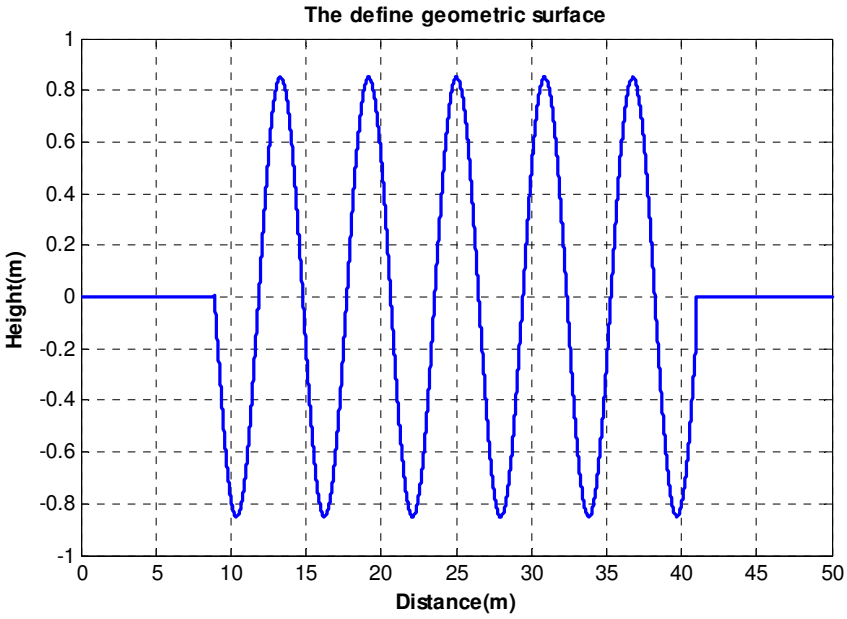

Figure 5. Cross-section of the sinusoidal surface defined using Matlab

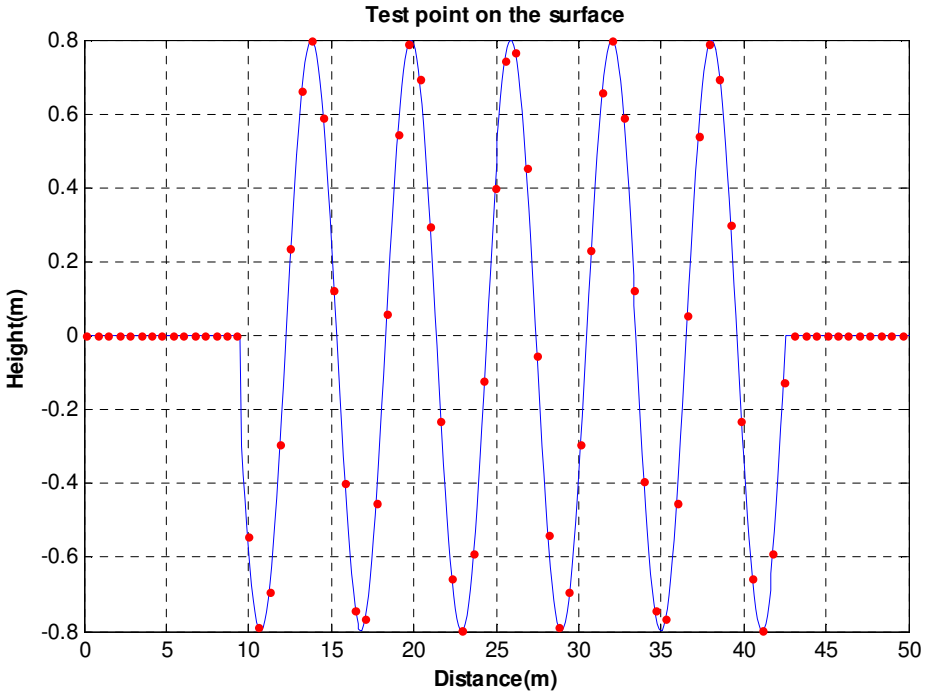

Figure 6. Defined interest points along the surface using Matlab

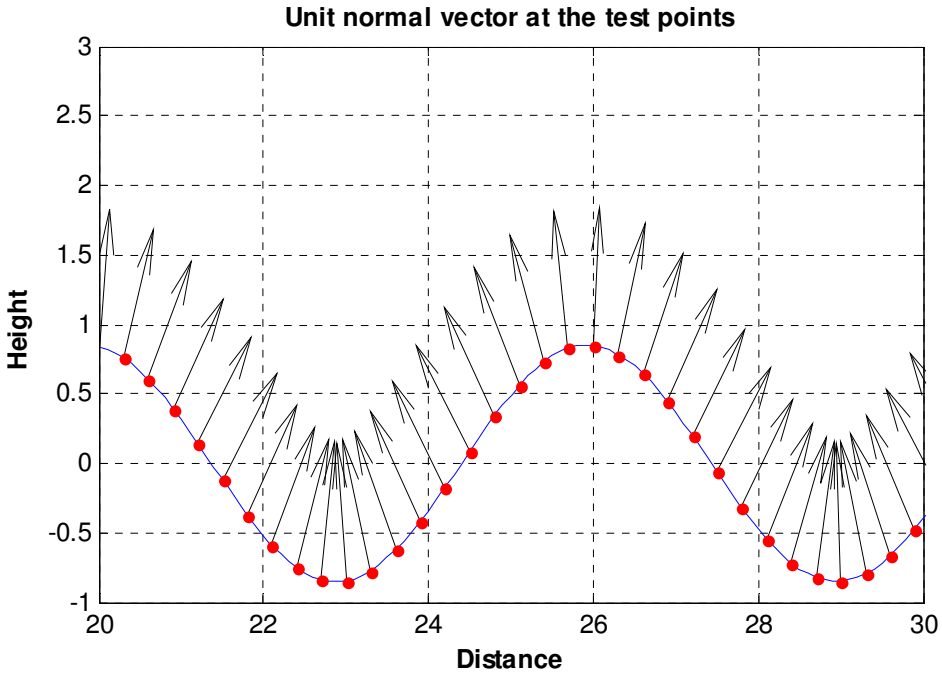

Figure 7. The unit normal vector at each interest point

4.2 Single Source Response Derivative

The response at the point of interest $r = (x, y)$ due to a single source at $r' = (x', y')$ is expressed as

$$G(r, r', k) = \frac{e^{\mathbf{j}kR}}{4\pi R} \tag{4. 10}$$

$$\text{where } R = ||r - r'|| = \sqrt{(x - x')^2 + (y - y')^2} \tag{4. 11}$$

The derivative of $G(r, r', k)$ with respect to x in Equation (4.10) is

$$\frac{\partial G(r, r', k)}{\partial x} = \frac{\partial G}{\partial R}\frac{\partial R}{\partial x}. \tag{4. 12}$$

where

$$\frac{\partial R}{\partial x} = \frac{(x - x')}{R}. \tag{4. 13}$$

Moreover

$$\begin{aligned}\frac{\partial G}{\partial R} &= \frac{\mathbf{j}ke^{\mathbf{j}kR}4\pi R}{(4\pi R)^2} - \frac{4\pi e^{\mathbf{j}kR}}{(4\pi R)^2} = \frac{\mathbf{j}ke^{\mathbf{j}kR}}{4\pi R} - \frac{e^{\mathbf{j}kR}}{4\pi R^2} \\ &= \frac{e^{\mathbf{j}kR}}{4\pi R}\left(-\frac{1}{R} + \mathbf{j}k\right). \end{aligned} \tag{4. 14}$$

Substituting Equation (4.13) and Equation (4.14) into Equation (4.12) yields

$$\frac{\partial G\left(r, r', k\right)}{\partial x} = \frac{e^{\mathbf{j}kR}\left(x - x'\right)}{4\pi R}\left(-\frac{1}{R^2} + \frac{\mathbf{j}k}{R}\right). \tag{4. 15}$$

Similarly, the derivative of $G\left(r, r', k\right)$ with respect to y is expressed as

$$\frac{\partial G\left(r, r', k\right)}{\partial y} = \frac{e^{\mathbf{j}kR}\left(y - y'\right)}{4\pi R}\left(-\frac{1}{R^2} + \frac{\mathbf{j}k}{R}\right). \tag{4. 16}$$

Equations (4.15) and (4.16) express the potential velocity used in the boundary condition.

4.3 Boundary Condition for a Single Source

The boundary condition at the points of interest r due to a single source at r' is expressed as

$$\psi\left(r, r', k\right) = \overrightarrow{n}\left(r\right) \cdot \nabla G\left(r, r', k\right). \tag{4. 17}$$

However, Equation (4.17) can be further written as

$$\psi\left(r, r', k\right) = \left[\frac{\partial G\left(r, r', k\right)}{\partial x}, \frac{\partial G\left(r, r', k\right)}{\partial y}\right]\begin{bmatrix}\cos\nu \\ \sin\nu\end{bmatrix}. \tag{4. 18}$$

Substituting Equations (4.15) and (4.16) into Equation (4.18) yields

$$\begin{aligned}\psi\left(r, r', k\right) &= \left[\frac{e^{\mathbf{j}kR_i}\left(x - x'\right)}{4\pi R}\left(-\frac{1}{R^2} + \frac{\mathbf{j}k}{R}\right), \frac{e^{\mathbf{j}kR_{ji}}\left(y_i - y'\right)}{4\pi R}\left(-\frac{1}{R^2} + \frac{\mathbf{j}k}{R}\right)\right] \\ &\quad \cdot \begin{bmatrix}\cos\nu \\ \sin\nu\end{bmatrix} \qquad (4.\ 19) \\ &= \frac{e^{\mathbf{j}kR}}{4\pi R}\left(-\frac{1}{R^2} + \frac{\mathbf{j}k}{R}\right)\left[\left(x - x'\right), \left(y - x'\right)\right] \cdot \begin{bmatrix}\cos\nu \\ \sin\nu\end{bmatrix}, \qquad (4.\ 20)\end{aligned}$$

then Equation (4.20) is further simplified into

$$\psi\left(r, r', k\right) = \frac{e^{\mathbf{j}kR}}{4\pi R}\left(-\frac{1}{R} + \mathbf{j}k\right)\frac{\left((x - x')\cos\nu + (y - y')\sin\nu\right)}{R} \tag{4. 21}$$

Equation (4.21) expresses the boundary condition at the points of interest over the geometric surface.

4.4 Main and Image Source Derivation

The pressure field at the point of interest r which is emanating from the two sources located at $s_H = (x_H, y_H)$ and $s_{-H} = (x_{-H}, y_{-H})$ is expressed as

$$\phi_{2H}\left(r, S_H, k\right) = \frac{e^{\mathbf{j}kR_H}}{4\pi R_H} + \frac{e^{\mathbf{j}kR_{-H}}}{4\pi R_{-H}} \tag{4. 22}$$

where R_H and R_{-H} are

$$R_H = \left|\left|\begin{bmatrix} x - x_H \\ y - y_H \end{bmatrix}\right|\right| = \left|\left|\begin{bmatrix} x \\ y - H \end{bmatrix}\right|\right| \tag{4. 23}$$

$$R_{-H} = \left|\left|\begin{bmatrix} x - x_{-H} \\ y - y_{-H} \end{bmatrix}\right|\right| = \left|\left|\begin{bmatrix} x \\ y + H \end{bmatrix}\right|\right| \tag{4. 24}$$

where H is the main source height from the flat surface and $x_H = x_{-H} = 0$. Figure (8) shows the condition for a completely flat surface.

The derivative of $\phi_{2H}\left(r, S_H, k\right)$ with respect to x is expressed as

$$\begin{aligned}\frac{\partial\phi_{2H}\left(r, S_H, k\right)}{\partial x} &= \frac{e^{\mathbf{j}kR_H}\left(x - x_H\right)}{4\pi R_H}\left(-\frac{1}{R_H^2} + \frac{\mathbf{j}k}{R_H}\right) \\ &\quad + \frac{e^{\mathbf{j}kR_2}\left(x - x_{-H}\right)}{4\pi R_{-H}}\left(-\frac{1}{R_{-H}^2} + \frac{\mathbf{j}k}{R_{-H}}\right).\end{aligned} \tag{4. 25}$$

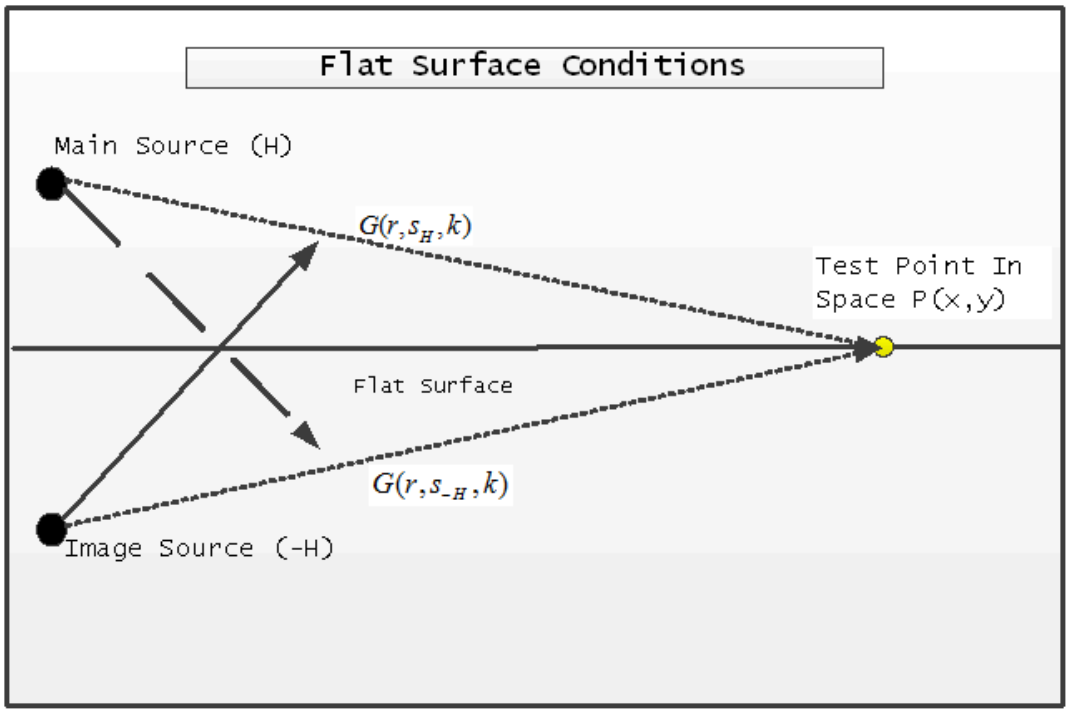

Figure 8. Modeling on a flat hard surface by placing two sources at the position s_H and s_{-H}.

Similarly the derivative of $\phi_{2H}(r, S_H, k)$ with respect to y is

$$\begin{aligned}\frac{\partial \phi_{2H}(r, S_H, k)}{\partial y} &= \frac{e^{\mathbf{j}kR_H}(y - y_H)}{4\pi R_H}\left(-\frac{1}{R_H^2} + \frac{\mathbf{j}k}{R_H}\right) \\ &\quad + \frac{e^{\mathbf{j}kR_{-H}}(y - y_{-H})}{4\pi R_{-H}}\left(-\frac{1}{R_{-H}^2} + \frac{\mathbf{j}k}{R_{-H}}\right).\end{aligned} \tag{4. 26}$$

The boundary condition for the pressure field $\phi_{2H}(r, S_H, k)$ is expressed as

$$\overrightarrow{n}(x) \cdot \nabla \phi_{2H}(r, S_H, k) = \overrightarrow{n}(x) \cdot \nabla G(r, s_H, k) + \overrightarrow{n}(x) \cdot \nabla G(r, s_{-H}, k) \tag{4. 27}$$

$$\psi_{2H} = \psi_H + \psi_{-H}. \tag{4. 28}$$

Thus ψ_H in Equation (4.28), which expresses the boundary condition at r due the main source s_H,

is

$$\psi_H = \overrightarrow{n}(x) \cdot \nabla G(r, s_H, k) \quad (4.\ 29)$$

$$= \frac{e^{\mathbf{j}kR_H}}{4\pi R_H}\left(-\frac{1}{R_H} + \mathbf{j}k\right)\frac{(x\cos\nu + (y-H)\sin\nu)}{R_H} \quad (4.\ 30)$$

and ψ_{-H} which expresses the boundary condition at r due the main source s_{-H} is

$$\psi_{-H} = \overrightarrow{n}(x) \cdot \nabla G(r, s_{-H}, k) \quad (4.\ 31)$$

$$= \frac{e^{\mathbf{j}kR_{-H}}}{4\pi R_{-H}}\left(-\frac{1}{R_{-H}} + \mathbf{j}k\right)\frac{(x\cos\nu + (y+H)\sin\nu)}{R_{-H}}. \quad (4.\ 32)$$

Therefore $\psi_{2H} = \psi_H + \psi_{-H}$ is expressed as

$$\psi_{2H} = \frac{e^{\mathbf{j}kR_H}}{4\pi R_H}\left(-\frac{1}{R_H} + \mathbf{j}k\right)\frac{(x\cos\nu + (y-H)\sin\nu)}{R_H} + \frac{e^{\mathbf{j}kR_{-H}}}{4\pi R_{-H}}\left(-\frac{1}{R_{-H}} + \mathbf{j}k\right)\frac{(x\cos\nu + (y+H)\sin\nu)}{R_{-H}}. \quad (4.\ 33)$$

Special Case: For the case where the surface is hard, flat, and horizontal, the distance between the main source position to the point of interest is equal to the distance from image source position to the same point of interest. The point of interest, the main, and the image sources position are defined as

$$r = \begin{bmatrix} x & 0 \end{bmatrix}^T, s_H = \begin{bmatrix} 0 & H \end{bmatrix}^T \text{ and } s_{-H} = \begin{bmatrix} 0 & -H \end{bmatrix}^T \quad (4.\ 34)$$

where the distances R_H and R_{-H} are expressed as

$$R_H = ||r - s_H|| = \sqrt{x^2 + H^2}, \quad (4.\ 35)$$

$$R_{-H} = ||r - s_{-H}|| = \sqrt{x^2 + H^2}. \quad (4.\ 36)$$

Thus

$$R_H = R_{-H} = R,\ \cos\nu = 0, \text{and}\ \sin\nu = 1. \tag{4. 37}$$

Substituting Equations (4.34) and (4.37) into Equation (4.25) yields

$$\frac{\partial\phi_{2H}\left(r, S_H, k\right)}{\partial x} = \frac{2e^{\mathbf{j}kR}x}{4\pi R}\left(-\frac{1}{R^2} + \frac{\mathbf{j}k}{R}\right). \tag{4. 38}$$

Similarly, after substituting Equations (4.34) and (4.37) into Equation (4.26), we have

$$\frac{\partial\phi_{2H}\left(r, S_H, k\right)}{\partial y} = 0. \tag{4. 39}$$

The boundary condition at the interest point located on a flat horizontal surface is expressed as

$$\begin{aligned}\psi_{\text{Flat}}\left(r, S, k\right) &= \overrightarrow{n}\left(x\right)\cdot\nabla\phi_{2H}^{\text{Flat}}\left(r, S, k\right)\\ &= \left[\frac{\partial\phi_{2H}\left(r, S_H, k\right)}{\partial x}, \frac{\partial\phi_{2H}\left(r, S_H, k\right)}{\partial y}\right]\left[\begin{array}{c}0\\1\end{array}\right] = 0\end{aligned} \tag{4. 40}$$

4.5 Multiple Source Derivatives

The pressure field $\phi\left(r_i, S, k\right)$ for a system containing more than two sources is expressed as

$$\phi\left(r_i, S, k\right) = A_H\phi_{2H}\left(r_i, S_H, k\right) + \sum_{j}^{N_s}\frac{A_j e^{\mathbf{j}kR_{ji}}}{4\pi R_{ji}}, \tag{4. 41}$$

where $\phi_{2H}\left(r_i, S_H, k\right)$ defines the pressure field due the two sources (main and image sources), N_s is the number of equivalent sources, A_j is the unknown complex amplitude of the equivalent sources and variable A_H is amplitude of the known main source. Figure (9) shows the location of the sources.

$$R_{ji} = ||r_i - s_j|| = \sqrt{\left(x_i - x_j\right)^2 + \left(y_i - y_j\right)^2} \tag{4. 42}$$

where R_{ji} is the distance between the interest points r_i to the equivalent sources at s_j. The

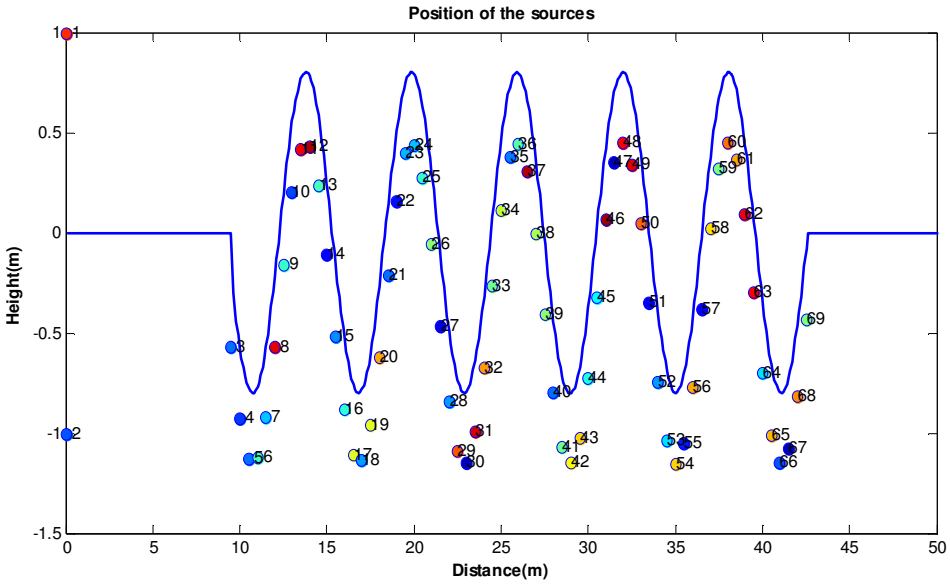

Figure 9. Every $0.5m$ there is an equivalent source $0.35m$ below the surface

boundary condition for the pressure field $\phi(r_i, S, k)$ in Equation (4.41) is expressed as

$$\psi(r_i, S, k) = \overrightarrow{n}(x_i) \cdot \nabla\phi(r_i, S, k). \tag{4. 43}$$

We substitute Equation (4.41) into Equation (4.43) to yield

$$\psi(r_i, S, k) = A_H \overrightarrow{n}(x_i) \cdot \nabla\phi_{2H}(r_i, S_H, k) + \sum_{j}^{N_s} A_j \overrightarrow{n}(x_i) \cdot \nabla G(r_i, s_j, k) \tag{4. 44}$$

where

$$G(r_i, s_j, k) = \frac{e^{\mathbf{j}kR_{ji}}}{4\pi R_{ji}}. \tag{4. 45}$$

However, the boundary condition for $G(r_i, s_j, k)$ is expressed by replacing r' with s_j and r with r_i in Equation (4.21). This leads to

$$\psi_{ji} = \nabla G(r_i, s_j, k) \cdot \overrightarrow{n}(x_i) \tag{4. 46}$$

$$= \frac{e^{\mathbf{j}kR_{ji}}}{4\pi R_{ji}} \left(-\frac{1}{R_{ji}} + \mathbf{j}k\right) \frac{((x_i - x_j)\cos\nu_i + (y_i - y_j)\sin\nu_i)}{R_{ji}}. \tag{4. 47}$$

In general, Equation (4.44) is expressed as

$$\psi\left(r_i, S, k\right) = A_H\left(\psi_{Hi} + \psi_{-Hi}\right) + \sum_{j}^{N_s} A_j \psi_{ji} \tag{4. 48}$$

where the relation

$$\psi_{Hi} + \psi_{-Hi} = \overrightarrow{n}\left(x_i\right) \cdot \nabla \phi_{2H}\left(r_i, S_H, k\right) \tag{4. 49}$$

$$\text{and } \psi_{ji} = \overrightarrow{n}\left(x_i\right) \cdot \nabla G\left(r_i, s_j, k\right) \tag{4. 50}$$

are expressed in Equation (4.27) and (4.46) respectively.

4.6 Ground Boundary Condition for an Unbounded Hard Surface

If the surface geometry of the ground is assumed to be hard, then the boundary condition $\psi\left(r_i, S, k\right)$ in Equation (4.48) is expressed as

$$0 = \psi\left(r_i, S, k\right) \tag{4. 51}$$

$$= A_H\left(\psi_{Hi} + \psi_{-Hi}\right) + \sum_{j}^{N_s} A_j \psi_{ji} \tag{4. 52}$$

with the complex amplitude A_j of the equivalent sources are unknown and variable A_H (complex amplitudes) is known. Equation (4.52) can be re-arranged as

$$\sum_{j}^{N_s} A_j \psi_{ji} = -A_H\left(\psi_{Hi} + \psi_{-Hi}\right) \tag{4. 53}$$

4.7 Least Square Estimate of the Equivalent Source Amplitude

For a system with a single point of interest r_1 and a multiple equivalent sources. The

complex amplitude A_j of the equivalent sources are compute as

$$\begin{bmatrix} \psi_{11} & \psi_{21} & \dots & \psi_{N_s1} \end{bmatrix} \begin{bmatrix} A_1 \\ A_2 \\ \vdots \\ A_{N_s} \end{bmatrix} = -A_H \left[\psi_{H1} + \psi_{-H1}\right]. \tag{4. 54}$$

Similarly for a system with several point of interest, Equation (4.54) is evaluated at each of the specified interest points over the undulating surface. Thus

$$\begin{bmatrix} \psi_{11} & \psi_{21} & \dots & \psi_{N_s1} \\ \psi_{12} & \psi_{22} & \dots & \psi_{N_s2} \\ \vdots & \vdots & \dots & \vdots \\ \psi_{1N_t} & \psi_{2N_t} & \dots & \psi_{N_sN_t} \end{bmatrix} \begin{bmatrix} A_1 \\ A_2 \\ \vdots \\ A_{N_s} \end{bmatrix} = -A_H \begin{bmatrix} \psi_{H1} + \psi_{-H1} \\ \psi_{H2} + \psi_{-H2} \\ \vdots \\ \psi_{HN_t} + \psi_{-HN_t} \end{bmatrix}, \tag{4. 55}$$

where N_t is the number of interest points on the surface. If the number of sources is less than the number of interest points on the surface $(N_s < N_t)$, then the total number of equations exceeds the total number of unknowns (Overdetermined System). Equation (4.55) can be written in the form $M\bar{a} = b$, where M represent the matrix at the left hand side of Equation (4.55), $\bar{a}$ represent the vector containing the unknown equivalent source complex amplitude and b represent the vector on the right hand side of the Equation (4.55)

$$b = -A_H \begin{bmatrix} \psi_{H1} + \psi_{-H1} \\ \psi_{H2} + \psi_{-H2} \\ \vdots \\ \psi_{HN_t} + \psi_{-HN_t} \end{bmatrix}. \tag{4. 56}$$

Hence

$$M\bar{a} = b. \tag{4. 57}$$

Using the least square method, $\bar{a}$ is solved for as follows

$$\bar{a} = \left(M^H M\right)^{-1} M^H b. \tag{4. 58}$$

4.8 Implementation of the Equivalent Source Method

The equivalent source method can be implemented in various computer languages. Figure

(10) shows the flowchart algorithm for implementing the ESM. The equivalent sources are placed beneath the surface. The number and locations of the equivalent sources determine the accuracy of our result. A system with more strategically placed sources will give a better result. The complex amplitudes of the equivalent sources are computed using the least square method.

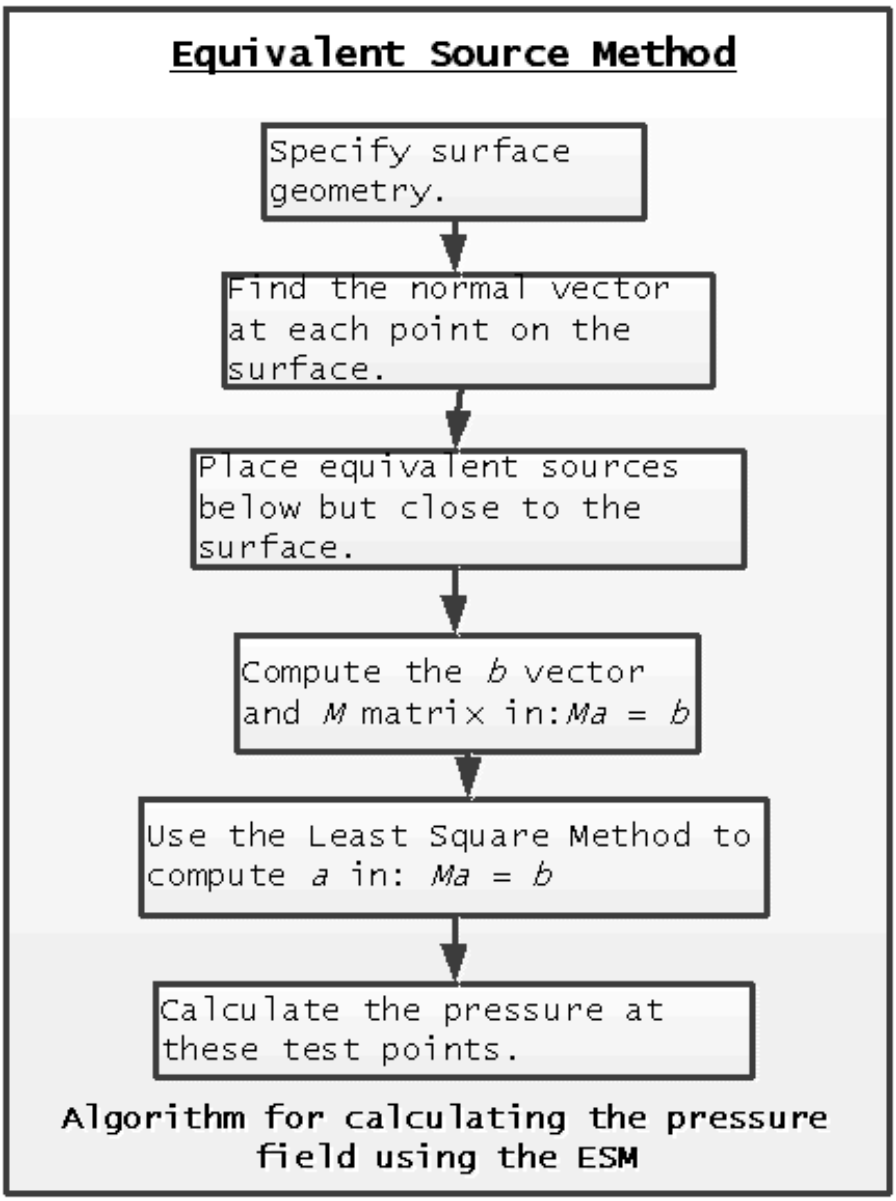

Figure 10. Computation of the pressure field using the ESM

4.9 Simulations

The complex amplitudes of the equivalent acoustic sources are estimated with the amplitude of the arbitrary main source given as $A_H = -130.99$ with excitation frequency defined as $f = 54.6$Hz which corresponds to the wavenumber $k = 1.1\text{m}^{-1}$. Simulation results are produced by the equivalent source method. Figure (11) displays the complex amplitude of the equivalent sources placed below the undulating surface.

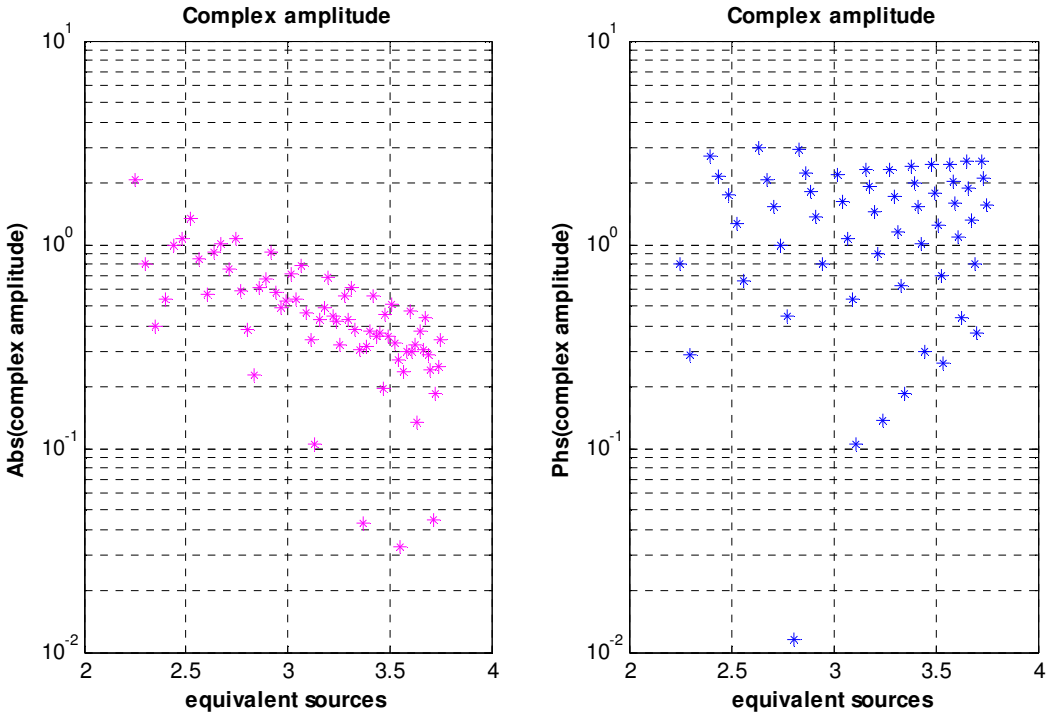

Figure 11. The magnitudes and the phase angles of the equivalent sources

Figure (12) shows the estimate of the acoustic loss, with the interest points located directly on the surface. Figure (13) shows the case where the interest points are located $1m$ above the undulating surface. Figure (14) shows the case where the interest points are located $1.5m$ above the undulating surface. Figure (15) shows the acoustic loss for interest points located on a horizontal line above the undulating surface. Figure (16) shows the pressure field where the

interest points are located $1m$ over the corrugation length of $100m$.

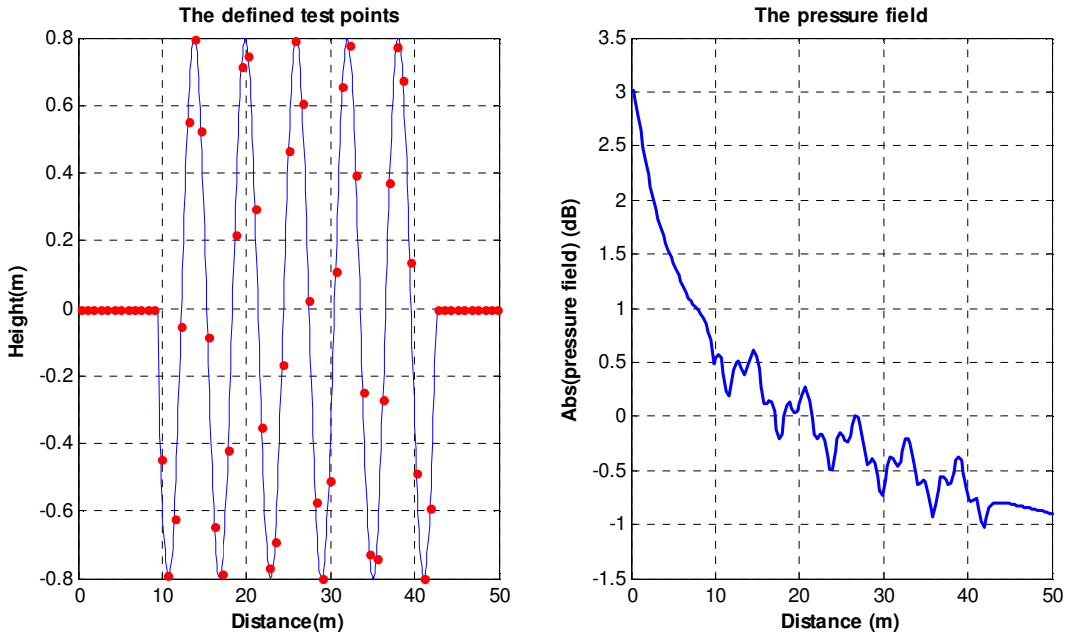

Figure 12. Pressure magnitude at points $x = 0.1m$ to $x = 50m$. The boundary condition is enforced on these test points.

Simulation with excitation frequency defined by $f = 78.6$Hz for the corrugation length of $50m$ and $100m$ is also examined. Figures (17), (18), (19) and (20) show the acoustic loss over the undulating surface. The results show that increasing the corrugation of the surfaces will result in a significant loss of the low-frequency as it propagates over the undulating surface.

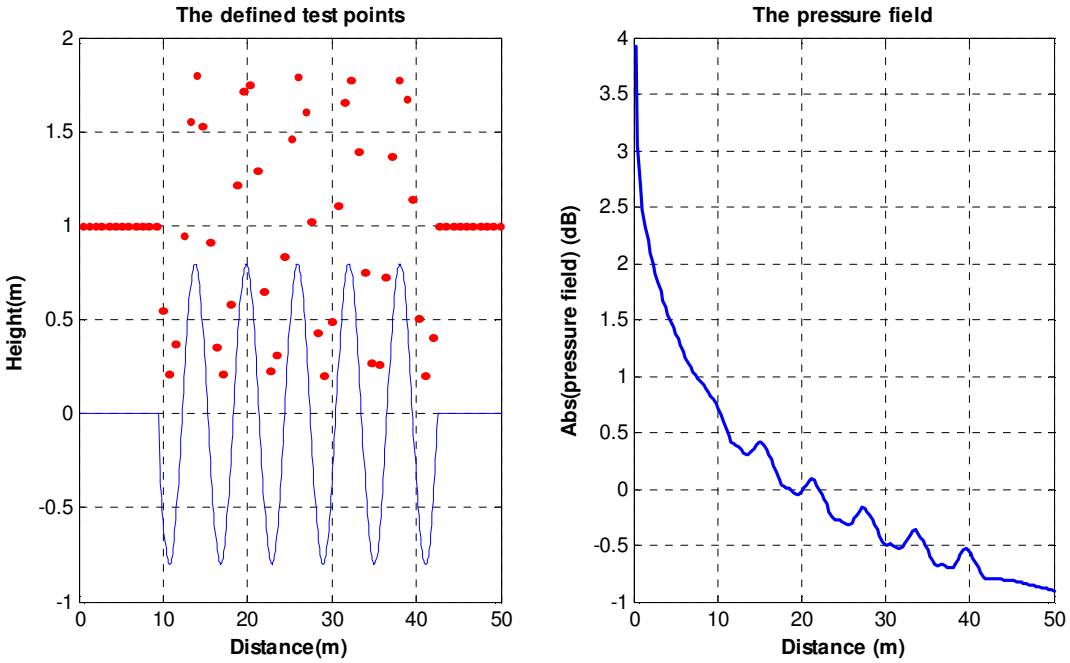

Figure 13. Pressure magnitude at points $x = 0.1m$ to $50m$ and $y = 1m$ above the surface.

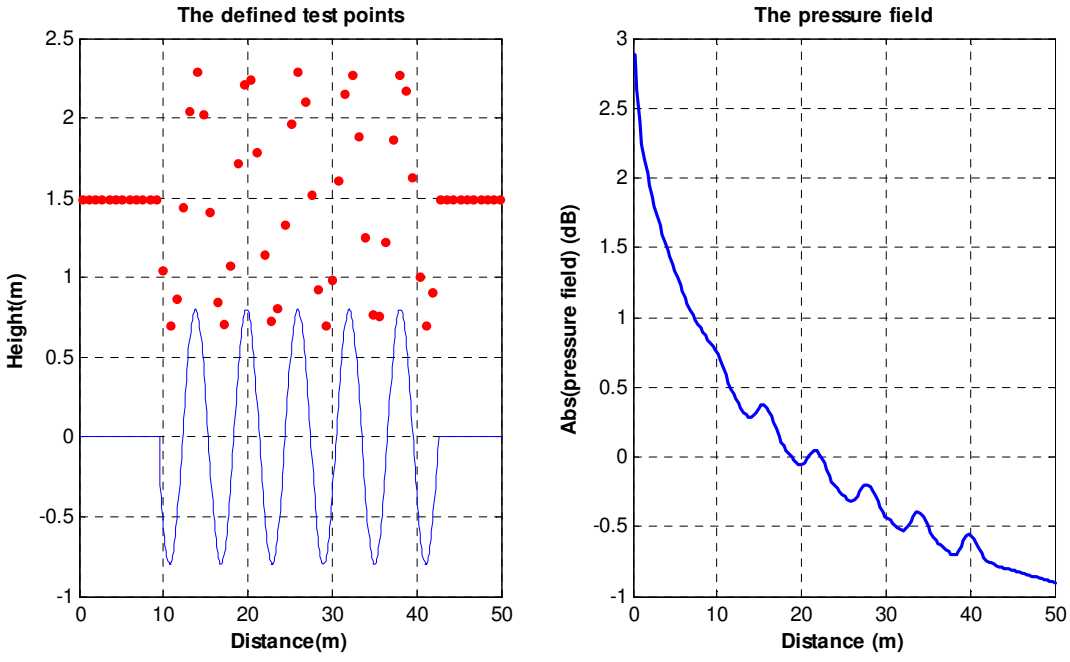

Figure 14. Pressure magnitude at points $x = 0.1m$ to $50m$ and $y = 1.5m$ above the surface.

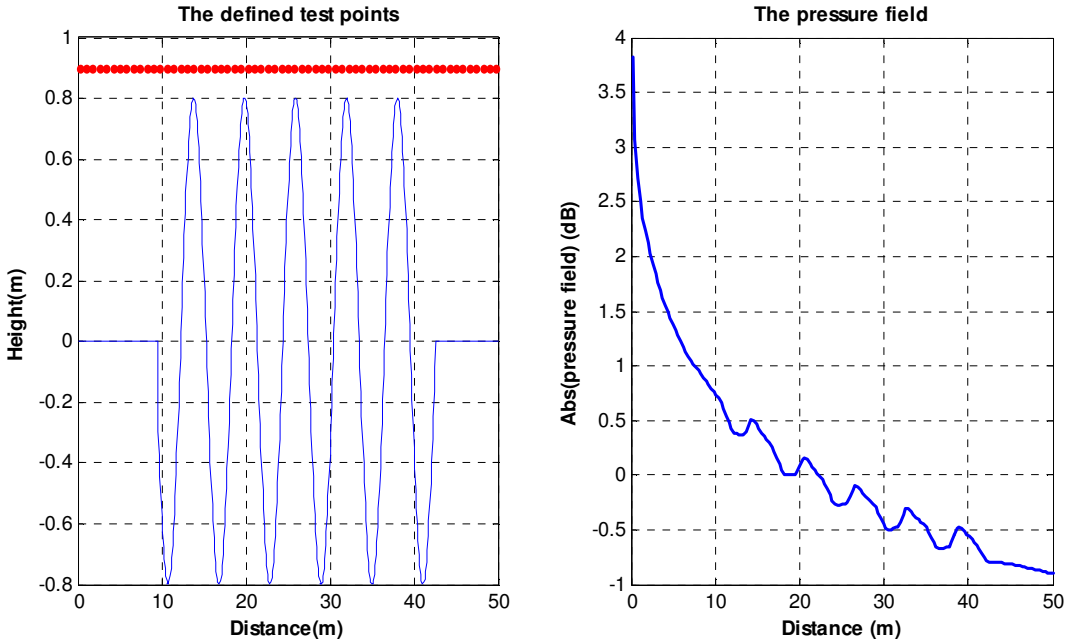

Figure 15. Pressure magnitude at points $x = 0.1m$ to $x = 50m$ and $y = 0.9m$.

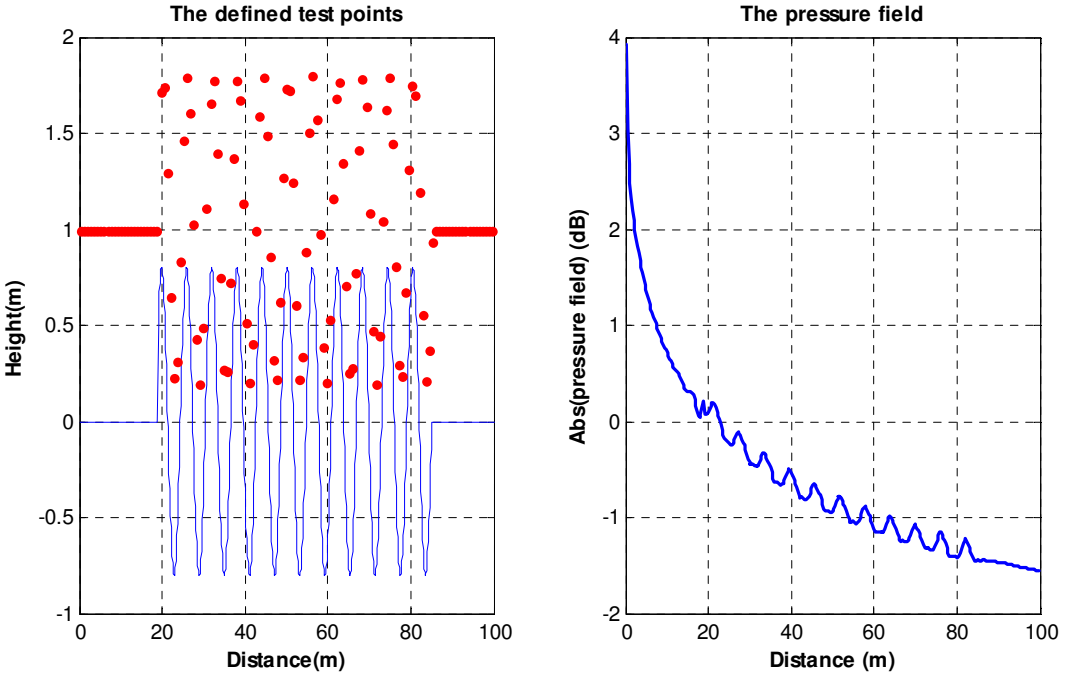

Figure 16. Pressure magnitude at points $x = 0.1m$ to $x = 100m$ at $y = 1m$ above the surface

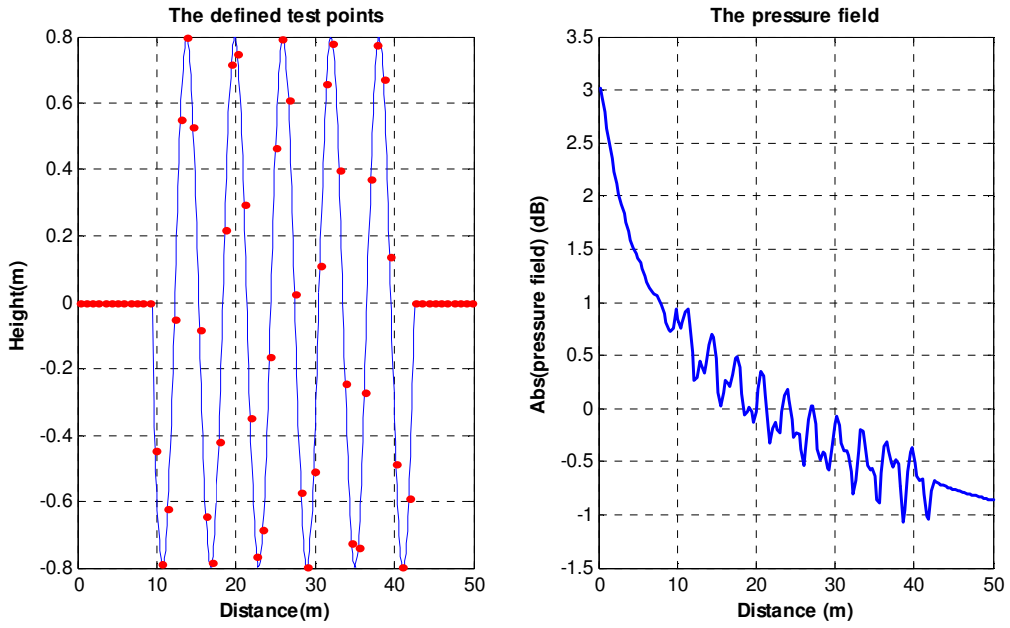

Figure 17. Pressure magnitude at points $x = 0.1m$ to $x = 50m$ with $k = 1.5m^{-1}$. The boundary condition is enforced on these test points.

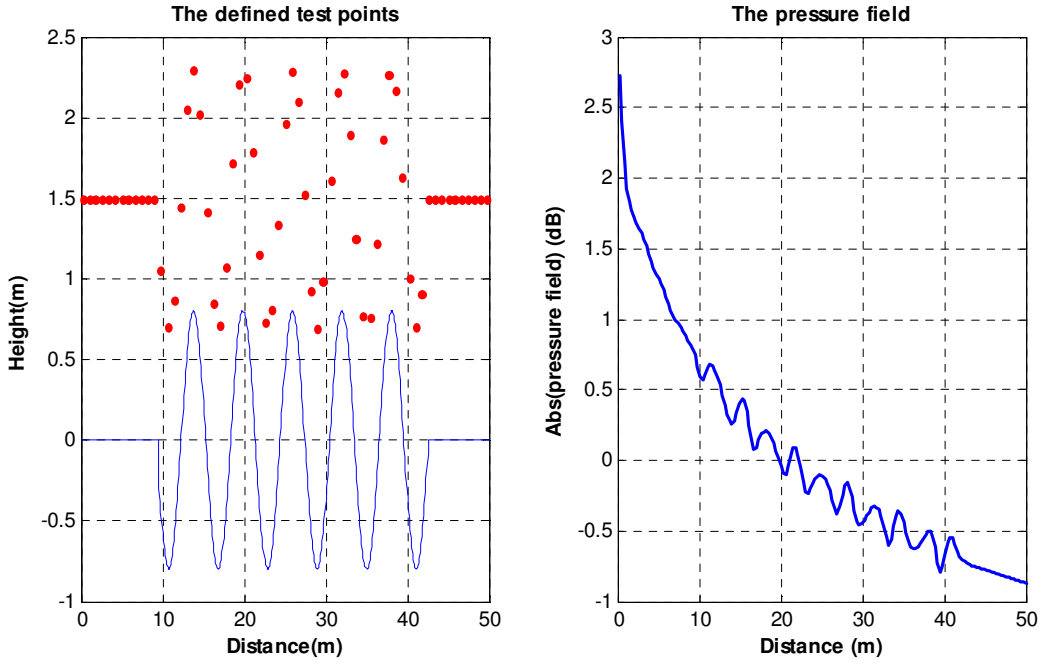

Figure 18. Pressure magnitude at points $x = 0.1m$ to $x = 50m$ and $y = 1.5m$ above the surface with $k = 1.5m^{-1}$.

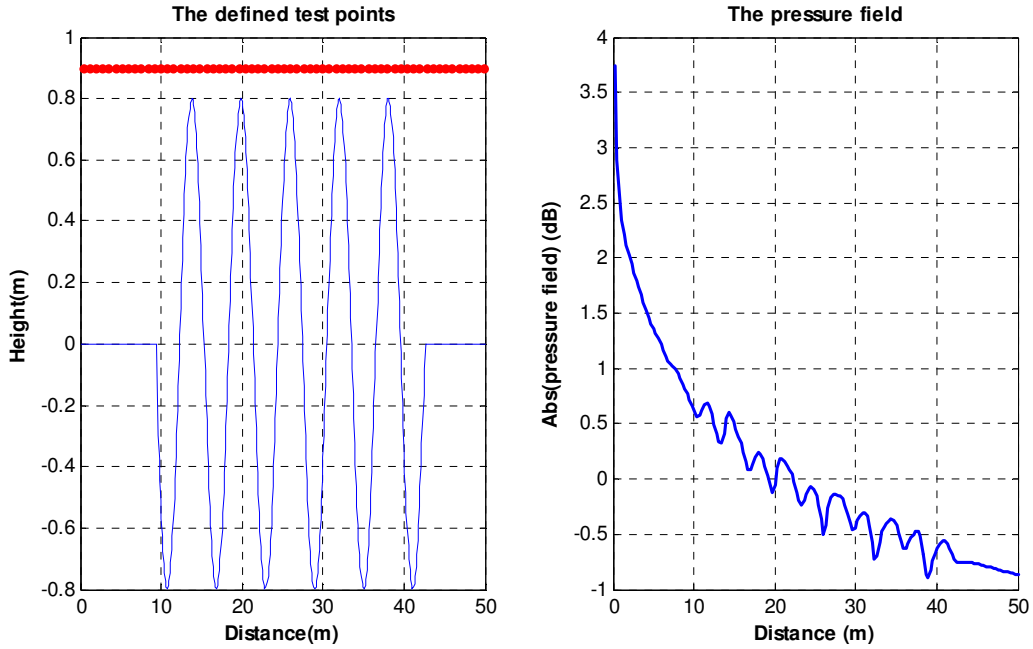

Figure 19. Pressure magnitude at points $x = 0.1m$ to $x = 50m$ and $y = 0.9m$ with $k = 1.5m^{-1}$.

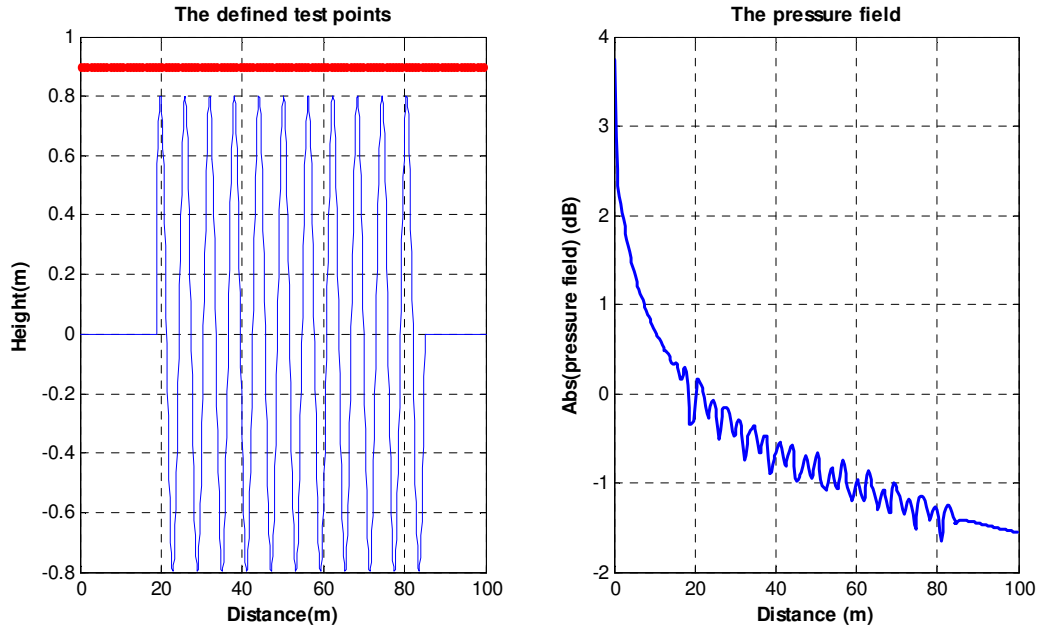

Figure 20. Pressure magnitude at points $x = 0.1m$ to $x = 100m$ and $y = 0.9m$ with $k = 1.5m^{-1}$.

CHAPTER 5

HARMONIC MODELING OVER A SOFT SURFACE USING COMPLEX EQUIVALENT SOURCES

In 2004, Ochmann [31] used the idea of superposition of the equivalent point sources, but to allow the sources to be located at complex positions to find the Green's function over impedance plane using the convergent integral. Deschamps [8] originally introduced this idea. Deschamps used complex source locations to model the propagation of a Gaussian beam. The corresponding field approximately behaves like a pulse at the paraxial region near the y axis. Ochmann's contribution of the impedance to the Green's function is given by

$$\mathcal{B}(r,H,k) = -\frac{k}{2\pi Z_0}\int_{-\infty}^{-H}\frac{e^{\mathbf{j}k\hat{R}}}{\hat{R}}e^{\frac{k}{Z_0}\varsigma}d\varsigma \tag{5. 1}$$

$$\text{for } -\infty < \varsigma \leq -H \quad (\varsigma \text{ real}) \tag{5. 2}$$

where

$$\hat{R} = \sqrt{x^2+(y+H-\mathbf{j}\varsigma)^2} \tag{5. 3}$$

Starting at the image source position $(0,-H)$ and adding infinitesimal sources along an imaginary position y axis at $y=-H+\mathbf{j}\varsigma$, the function $\mathcal{B}(r,H,k)$ defines the response in space due to the sources paraxial to $-H$. The pressure field $\phi_{2H}(r_i,S,k)$ for a completely flat horizontal soft surface is given by

$$\phi_{2H}(r,S_H,k) = \frac{e^{\mathbf{j}kR_H}}{4\pi R_H}+\frac{e^{\mathbf{j}kR_{-H}}}{4\pi R_{-H}}+\mathcal{B}(r,H,k). \tag{5. 4}$$

This approach has enormous advantages in that the line integral in Equation (5.1) convergence for all surface impedances whose real part are positive. In this case, the kernel of the integral decays exponentially.

5.1 Derivatives of the Soft-Contributing Green's Function

The derivative of $\mathcal{B}(r, H, k)$ in Equation (5.1) with respect to x is expressed as

$$\frac{\partial \mathcal{B}(r, H, k)}{\partial x} = \frac{\partial \mathcal{B}(r, H, k)}{\partial \hat{R}} \frac{\partial \hat{R}}{\partial x} \tag{5. 5}$$

where the derivative of $\frac{e^{\mathbf{j}k\hat{R}}}{\hat{R}}$ with respect to $\hat{R}$ is

$$\frac{\partial}{\partial \hat{R}} \left(\frac{e^{\mathbf{j}k\hat{R}}}{\hat{R}} \right) = \frac{\mathbf{j}e^{\mathbf{j}k\hat{R}} \left(\mathbf{j} + k\hat{R} \right)}{\hat{R}^2}, \tag{5. 6}$$

$$\frac{\partial \hat{R}}{\partial x} = \frac{x}{\hat{R}}. \tag{5. 7}$$

In short, Equation (5.5) is expressed as

$$\frac{\partial \mathcal{B}(r, H, k)}{\partial x} = -\frac{k}{2\pi Z_0} \int_{-\infty}^{-H} \frac{\mathbf{j}e^{\mathbf{j}k\hat{R}} \left(\mathbf{j} + k\hat{R} \right) x}{\hat{R}^3} e^{\frac{k}{Z_0}\varsigma} d\varsigma. \tag{5. 8}$$

Similarly, the derivative of $\mathcal{B}(r, H, k)$ with respect to y

$$\frac{\partial \mathcal{B}(r, H, k)}{\partial y} = \frac{\partial \mathcal{B}(r, H, k)}{\partial \hat{R}} \frac{\partial \hat{R}}{\partial y}, \tag{5. 9}$$

$$\frac{\partial \hat{R}}{\partial y} = \frac{y + H - \mathbf{j}\varsigma}{\hat{R}} \tag{5. 10}$$

thus

$$\frac{\partial \mathcal{B}(r, H, k)}{\partial y} = -\frac{k}{2\pi Z_0} \int_{-\infty}^{-H} \frac{\mathbf{j}e^{\mathbf{j}k\hat{R}} \left(\mathbf{j} + k\hat{R} \right) (y + H - \mathbf{j}\varsigma)}{\hat{R}^3} e^{\frac{k}{Z_0}\varsigma} d\varsigma \tag{5. 11}$$

Equations (5.8) and (5.11) express the derivatives used in the boundary conditions. The boundary condition of $\mathcal{B}(r_i, H, k)$ for a system with multiple interest points r_i is expressed as

$$\beta_i = \overrightarrow{n}(x_i) \cdot \nabla \mathcal{B}(r_i, H, k). \tag{5. 12}$$

Thus Equation (5.12) is written as

$$\beta_i = \left[\frac{\partial \mathcal{B}\left(r_i, H, k\right)}{\partial x}, \frac{\partial \mathcal{B}\left(r_i, H, k\right)}{\partial y} \right] \begin{bmatrix} \cos\nu_i \\ \sin\nu_i \end{bmatrix}. \tag{5. 13}$$

Substituting Equations (5.8) and (5.11) into Equations (5.13) yields

$$\beta_i = -\frac{k}{2\pi Z_0} \int_{-\infty}^{-H} \left(\frac{\mathbf{j} e^{\mathbf{j}k\hat{R}_i} \left(\mathbf{j} + k\hat{R}_i\right) e^{\frac{k}{Z_0}\varsigma}}{\hat{R}_i^3} \left(x_i \cos\nu_i + \left(y_i + H - \mathbf{j}\varsigma\right)\sin\nu_i\right) \right) d\varsigma \tag{5. 14}$$

Equations (5.14) expresses the contribution of the plane impedance to the boundary condition at any point of interest on the geometric surface.

5.2 Multiple Sources over an Undulating Soft Surface

The pressure field $\phi\left(r_i, S, k\right)$ for a system containing more than two sources is expressed as

$$\phi\left(r_i, S, k\right) = A_H \phi_{2H}\left(r_i, S_H, k\right) + A_H \mathcal{B}\left(r_i, H, k\right) + \sum_{j}^{N_s} \frac{A_j e^{\mathbf{j}kR_{ji}}}{4\pi R_{ji}}. \tag{5. 15}$$

The boundary condition for $\phi\left(r_i, S, k\right)$ in Equation (5.15) is expressed as

$$\psi\left(r_i, s_j, k\right) = \overrightarrow{n}\left(x_i\right) \cdot \nabla\phi\left(r_i, S, k\right). \tag{5. 16}$$

Substituting Equation (5.15) into Equation (5.16) yields

$$\begin{aligned} \psi\left(r_i, S, k\right) &= A_H \overrightarrow{n}\left(x_i\right) \cdot \nabla\phi_{2H}\left(r_i, S_H, k\right) + A_H \overrightarrow{n}\left(x_i\right) \cdot \nabla\mathcal{B}\left(r_i, H, k\right) \\ &\quad + \sum_{j}^{N_s} A_j \overrightarrow{n}\left(x_i\right) \cdot \nabla G\left(r_i, s_j, k\right). \end{aligned} \tag{5. 17}$$

A collection of all the terms transforms Equation (5.17) into

$$\psi\left(r_i, s_j, k\right) = A_H\left(\psi_{Hi} + \psi_{-Hi}\right) + A_H\beta_i + \sum_{j}^{N_s} A_j \psi_{ji}, \tag{5. 18}$$

where

$$\begin{aligned}\psi_{Hi}+\psi_{-Hi} &= \overrightarrow{n}(x_i)\cdot\nabla\phi_{2H}(r_i,S_H,k),\\ \psi_{ji} &= \overrightarrow{n}(x_i)\cdot\nabla G(r_i,s_j,k),\\ \beta_i &= \overrightarrow{n}(x_i)\cdot\nabla\mathcal{B}(r_i,H,k),\end{aligned}$$

are expressed in Equations (4.27) and (4.44) and (5.14) respectively.

5.3 Ground Boundary Condition for an Unbounded Soft Surface

The boundary condition $\psi(r_i,s_j,k)$ in Equation (5.18) for a soft surface is expressed as

$$\psi(r_i,S,k)=-\frac{\mathbf{j}k}{Z_0}\phi(r_i,S,k), \tag{5.19}$$

where the right hand side of Equation (5.19) is simplified as

$$\begin{aligned}\frac{\mathbf{j}k}{Z_0}\phi(r_i,S,k) &= A_H\frac{\mathbf{j}k}{Z_0}\left[G(r_i,s_H,k)+G(r_i,s_{-H},k)+\mathcal{B}(r_i,H,k)\right]\\ &\quad+\frac{\mathbf{j}k}{Z_0}\sum_{j}^{N_s}A_jG(r_i,s_j,k).\end{aligned} \tag{5.20}$$

The terms in Equation (5.20) are expressed as

$$\bar{G}_{Hi} = \frac{\mathbf{j}k}{Z_0}G(r_i,s_H,k) \text{ and } \bar{G}_{-Hi}=\frac{\mathbf{j}k}{Z_0}G(r_i,s_{-H},k), \tag{5.21}$$

$$\bar{G}_{ji} = \frac{\mathbf{j}k}{Z_0}G(r_i,s_j,k) \text{ and } \bar{\mathcal{B}}_i=\frac{\mathbf{j}k}{Z_0}\mathcal{B}(r_i,H,k). \tag{5.22}$$

Thus Equation (5.20) becomes

$$-\frac{\mathbf{j}k}{Z_0}\phi(r_i,S,k)=-A_H\left(\bar{G}_{Hi}+\bar{G}_{-Hi}+\bar{\mathcal{B}}_i\right)-\sum_{j}^{N_s}A_j\bar{G}_{ji}. \tag{5.23}$$

Equation (5.19) becomes

$$0 = A_H \left(\psi_{Hi} + \psi_{-Hi} + \bar{G}_{Hi} + \bar{G}_{-Hi} + \beta_i + \bar{\mathcal{B}}_i\right) + \sum_j^{N_s} A_j \left(\psi_{ji} + \bar{G}_{ji}\right). \tag{5. 24}$$

The complex amplitude A_j of the equivalent sources are unknown and variable, but A_H (complex amplitude of the main source) is known. Equation (5.24) is re-arranged as

$$\sum_j^{N_s} A_j \left(\psi_{ji} + \bar{G}_{ji}\right) = -A_H \left(\psi_{Hi} + \psi_{-Hi} + \bar{G}_{Hi} + \bar{G}_{-Hi} + \beta_i + \bar{\mathcal{B}}_i\right) \tag{5. 25}$$

5.4 Least Square Estimate of the Equivalent Source Amplitude

For a system with single interest point and multiple equivalent sources, the complex amplitudes A_j expressed in Equation (5.25) must satisfy

$$\begin{aligned} &\begin{bmatrix} \psi_{11} + \bar{G}_{11} & \psi_{21} + \bar{G}_{21} & \ldots & \psi_{N_s1} + \bar{G}_{N_s1} \end{bmatrix} \begin{bmatrix} A_1 \\ A_2 \\ \vdots \\ A_{N_s} \end{bmatrix} \\ = \;& -A_H \left[\psi_{H1} + \psi_{-H1} + \bar{G}_{H1} + \bar{G}_{-H1} + \beta_1 + \bar{\mathcal{B}}_1\right]. \end{aligned} \tag{5. 26}$$

In the case of several points of interest over an undulating surface, the right hand side of Equation (5.26) is expressed as

$$b = -A_H \begin{bmatrix} \psi_{H1} + \psi_{-H1} + \bar{G}_{H1} + \bar{G}_{-H1} + \beta_1 + \bar{\mathcal{B}}_1 \\ \psi_{H2} + \psi_{-H2} + \bar{G}_{H2} + \bar{G}_{-H2} + \beta_2 + \bar{\mathcal{B}}_2 \\ \vdots \\ \psi_{HN_t} + \psi_{-HN_t} + \bar{G}_{HN_t} + \bar{G}_{-HN_t} + \beta_{N_t} + \bar{\mathcal{B}}_{N_t} \end{bmatrix}, \tag{5. 27}$$

and the left hand side matrix is expressed as

$$\begin{bmatrix} \psi_{11} & \psi_{21} & \ldots & \psi_{N_s1} \\ \psi_{12} & \psi_{22} & \ldots & \psi_{N_s2} \\ \vdots & \vdots & \ldots & \vdots \\ \psi_{1N_t} & \psi_{2N_t} & \ldots & \psi_{N_sN_t} \end{bmatrix} = M_1 \text{ and } \begin{bmatrix} \bar{G}_{11} & \bar{G}_{21} & \ldots & \bar{G}_{N_s1} \\ \bar{G}_{12} & \bar{G}_{22} & \ldots & \bar{G}_{N_s2} \\ \vdots & \vdots & \ldots & \vdots \\ \bar{G}_{1N_t} & \bar{G}_{2N_t} & \ldots & \bar{G}_{N_sN_t} \end{bmatrix} = M_2, \tag{5. 28}$$

and $\hat{a}$ represent the vector containing the unknown complex amplitude

$$\begin{bmatrix} A_1 \\ A_2 \\ \vdots \\ A_{N_s} \end{bmatrix} = \hat{a}. \tag{5. 29}$$

Equation (5.26) is assembled as

$$(M_1 + M_2)\,\hat{a} = b. \tag{5. 30}$$

Using the least square method, $\hat{a}$ is computed as follows

$$\hat{a} = \Big((M_1 + M_2)^H (M_1 + M_2)\Big)^{-1} (M_1 + M_2)^H b \tag{5. 31}$$

5.5 Simulations

The amplitude of the arbitrary main source is $A_H = -130.99$, the impedance Z_0 is considered as 1 and the excitation frequency is $f = 54.6$Hz. Figure (21) displays the complex amplitude of the equivalent sources placed below the undulating surface. Because of the soft nature of the undulating surface, the sound pressure that is lost due to the impedance conditions is found to be twice that of a rigid surface.

Figure (22) shows the estimate of the acoustic sources, with the interest points located directly on the surface. Figure (23) shows the case where the interest points are located $1m$ above the undulating surface. Figure (24) shows the case where the interest points are located $1.5m$ above the undulating surface. Figure (25) shows the acoustic loss for an interest points are located horizontal above the undulating surface. Figure (26) shows the pressure field where the interest points are located $1m$ over the corrugation length of $100m$.

Simulation with excitation frequency defined as $f = 78.6$Hz for the corrugation length of $50m$ and $100m$ is also examined. Figures (27), (28), (29) and (30) illustrates the acoustic loss

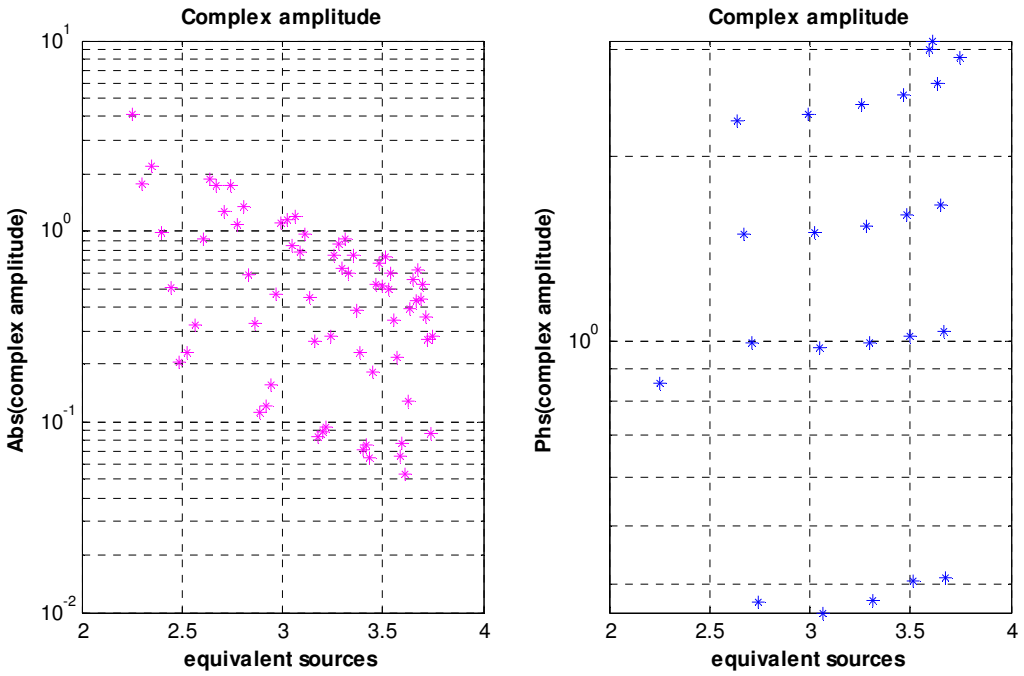

Figure 21. Magnitudes and phase angles of the equivalent source amplitudes below a soft surface.

over the undulating surface. The results show that increasing the length of the corrugation of the surface will result in a significant loss of the low-frequency as it propagates over the surface. This loss is estimated to be about 1 dB for a change of about 1/2 octave of frequency change.

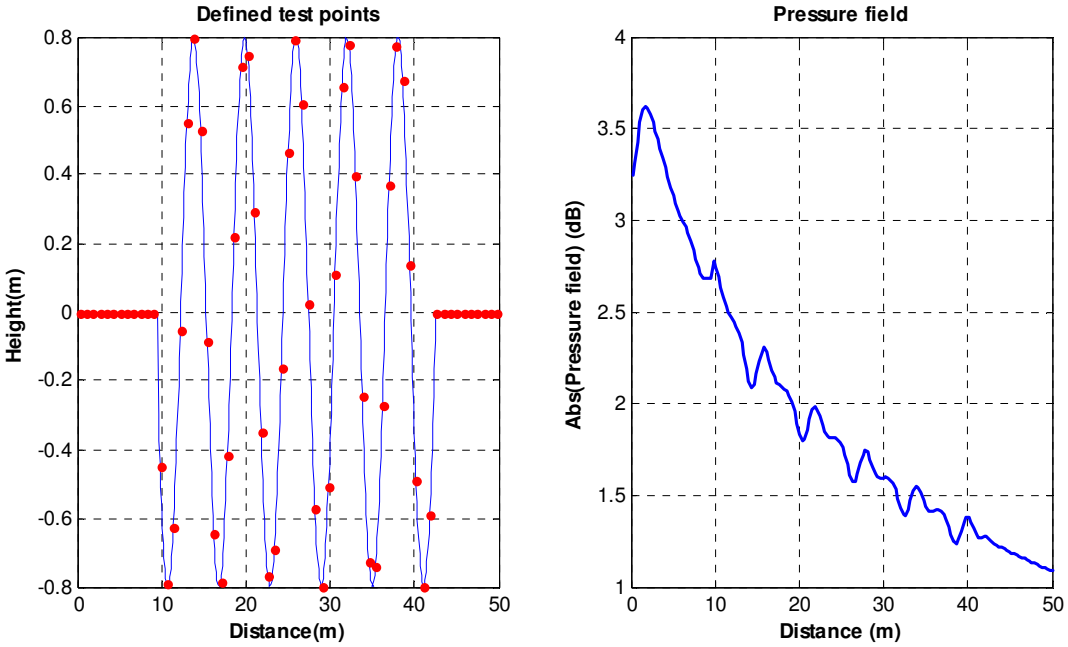

Figure 22. Pressure magnitude at points $x = 0.1m$ to $x = 50m$ over soft surface. The boundary condition is enforced on these test points.

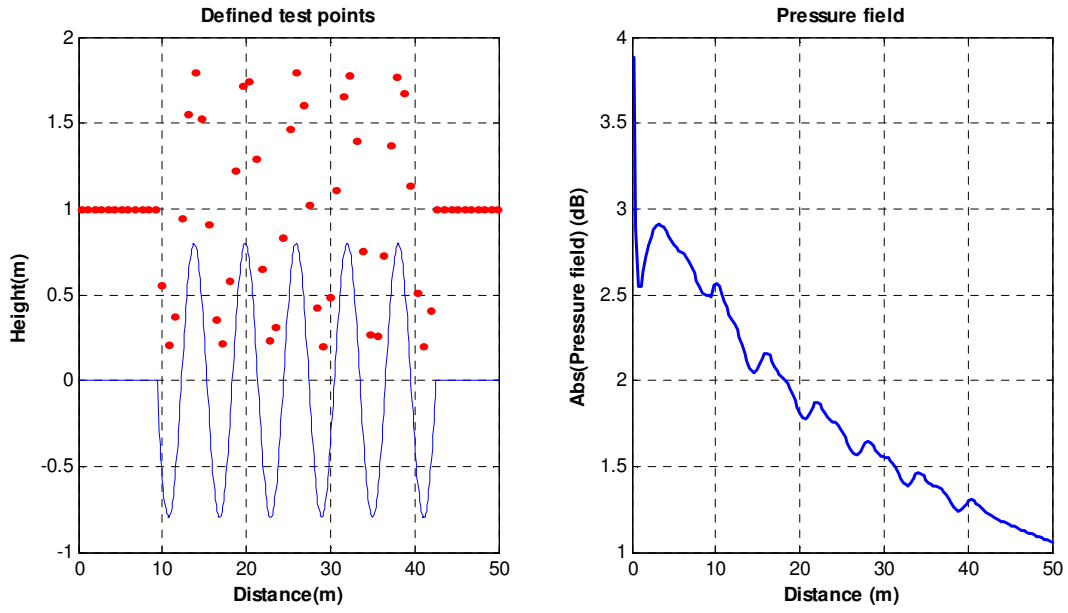

Figure 23. Pressure magnitude at points $x = 0.1m$ to $x = 50m$ and $y = 1m$ above the soft surface

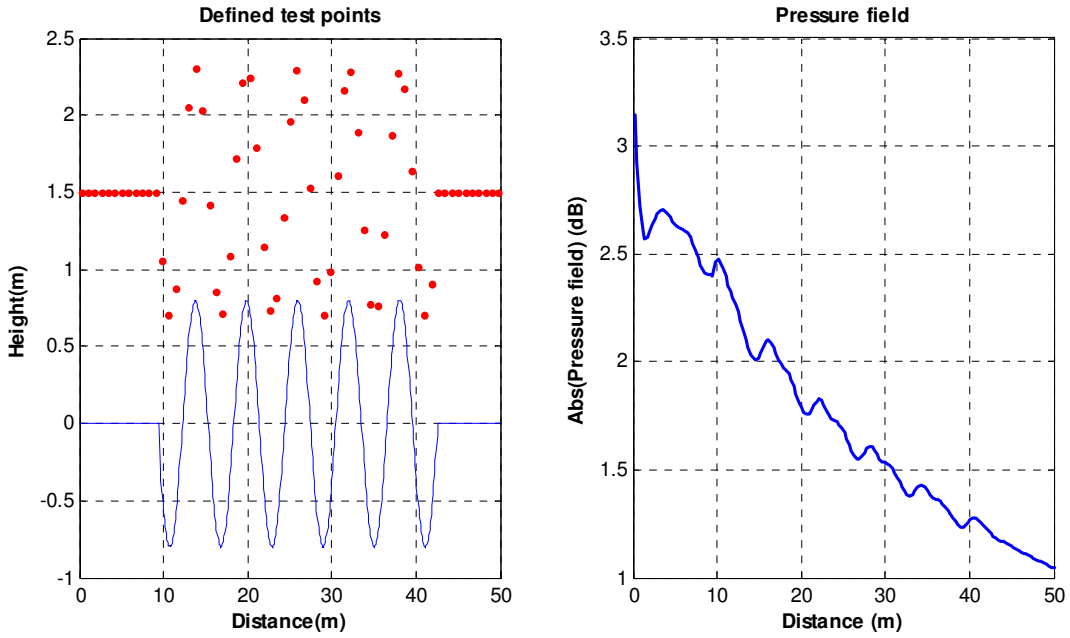

Figure 24. Pressure magnitude at points $x = 0.1m$ to $x = 50m$ and $y = 1.5m$ above the soft surface

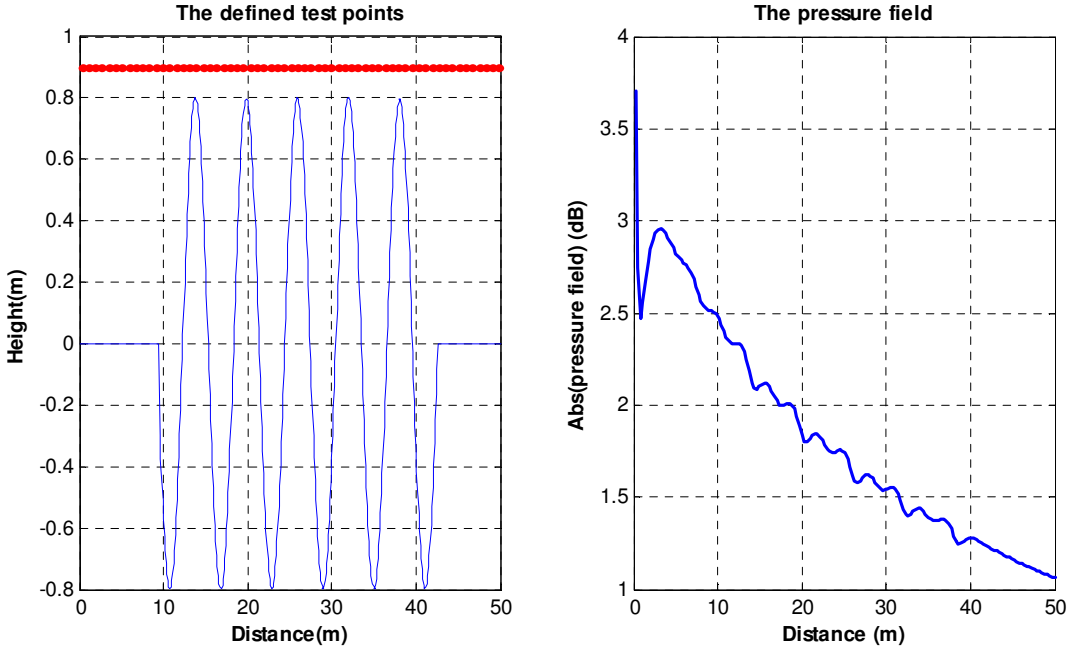

Figure 25. Pressure magnitude at points $x = 0.1m$ to $x = 50m$ and $y = 0.9m$.

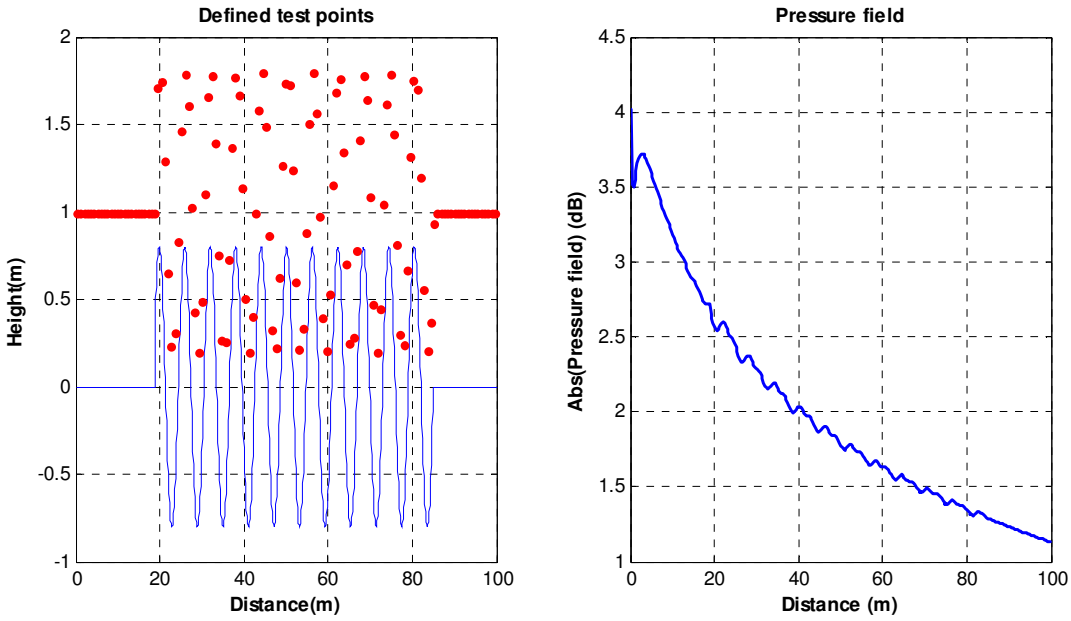

Figure 26. Pressure magnitude at points $x = 0.1m$ to $x = 100m$ and $y = 1m$ above the soft surface

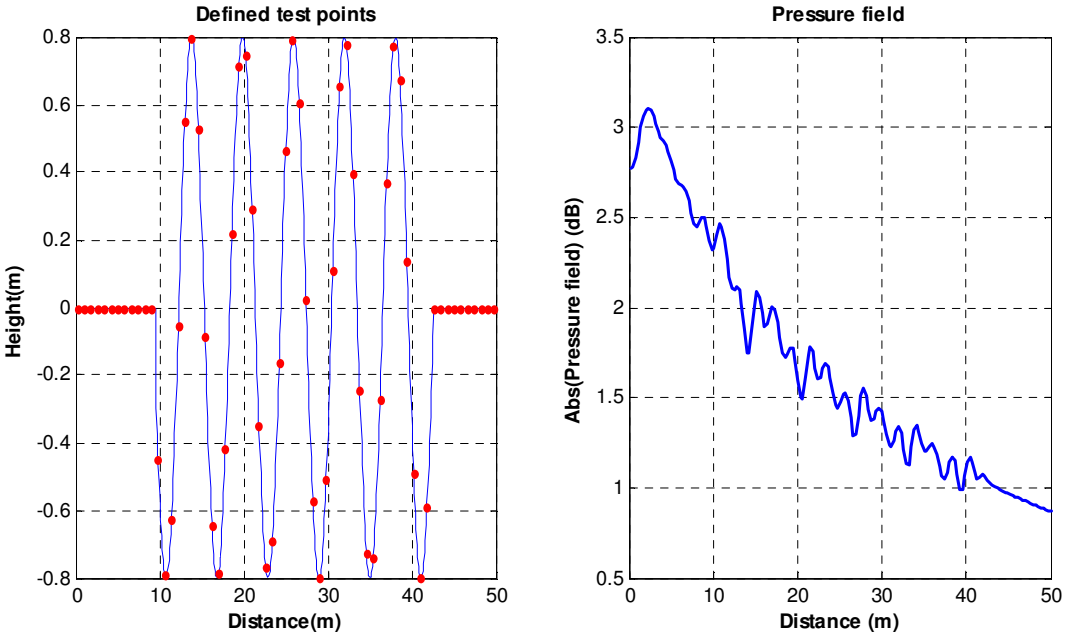

Figure 27. Pressure magnitude at points $x = 0.1m$ to $x = 50m$ over soft surface, with $k = 1.5m^{-1}$. The boundary condition is enforced on these test points.

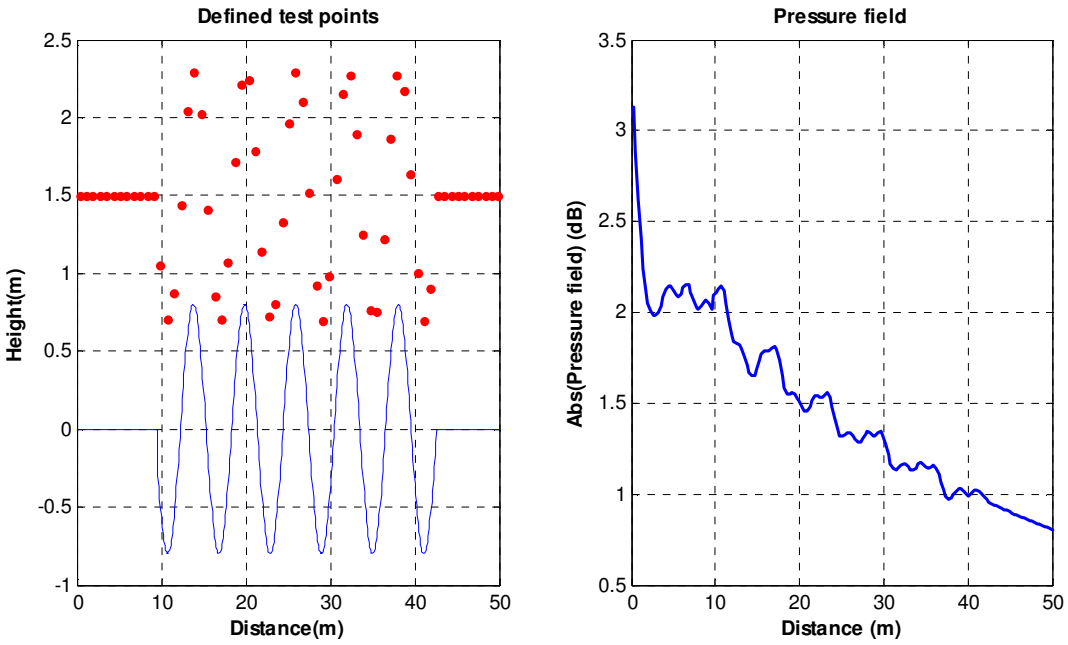

Figure 28. Pressure magnitude at points $x = 0.1m$ to $x = 50m$ and $y = 1.5m$ above the soft surface, with $k = 1.5m^{-1}$. The field is computed at these test points.

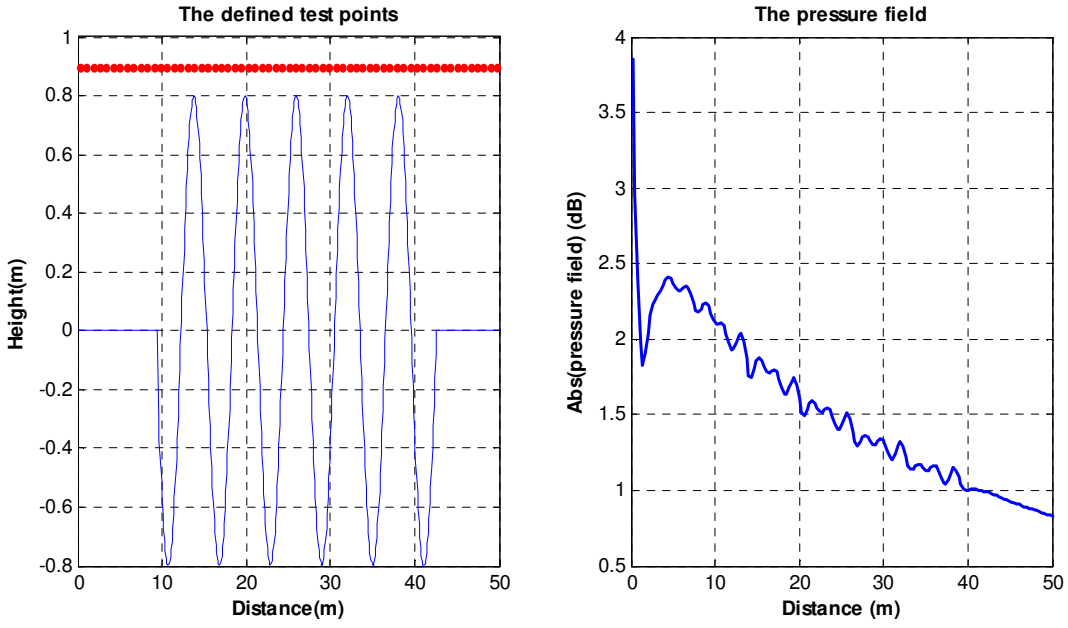

Figure 29. Pressure magnitude at points $x = 0.1m$ to $x = 50m$ and $y = 0.9m$, with $k = 1.5m^{-1}$ over a soft surface

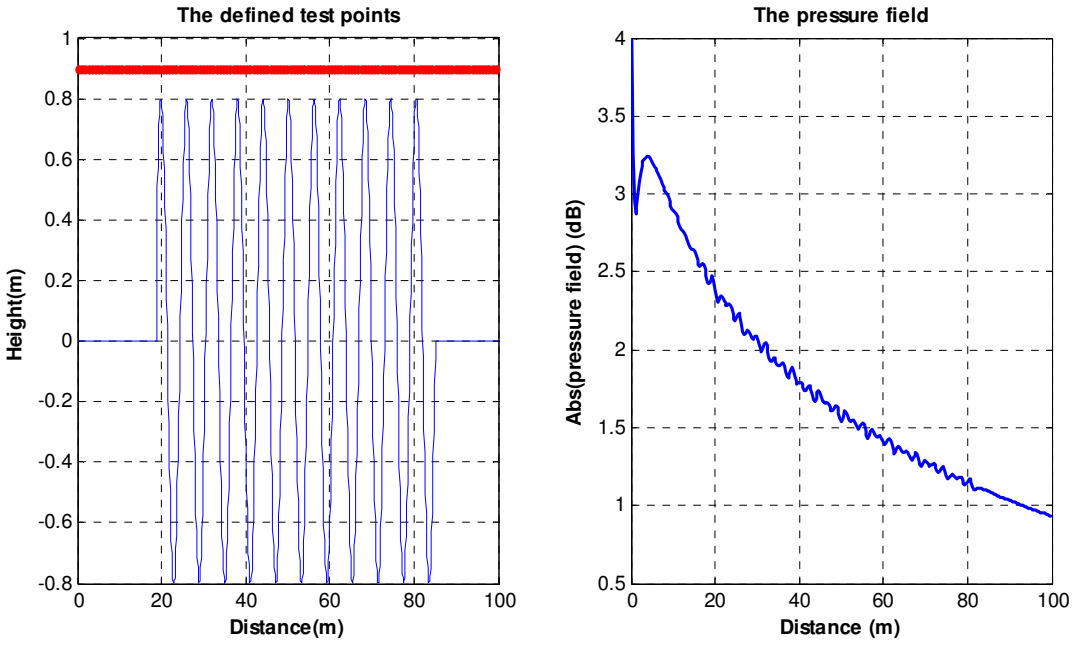

Figure 30. Pressure magnitude at points $x = 0.1m$ to $x = 100m$ and $y = 0.9m$ with $k = 1.5m^{-1}$ over a soft surface

CHAPTER 6

CONCLUSIONS

The wave acoustic wave propagating over an unbounded undulating outdoor surface is derived. Green's function for unbounded space is used to derive the responses to a Gaussian pulse and to harmonic source. Representing the effect of undulation by a set of equivalent sources just below the surface and combining the free-space Green's functions due to these sources allows us to represent the acoustic field faraway without having to solve a finite element problem. The complex amplitudes of the equivalent sources are solved by enforcing the boundary condition at a predetermined number of test points on the surface. We showed that a flat hard surface can be molded by placing the mirror of the main sources at the same height along the x-axis. We used Ochmann's approximation of the impedance contribution to derive a similar least-squares problem for an undulating soft surface.

We used the equivalent source method to model the acoustic transmission loss over an undulating boundary condition. The complex amplitudes of these equivalent sources are estimated using the least square method. For the case where the undulating surface is hard, with wavelength of $6.067m$, amplitude of $0.8m$, the first resonance occurs at 54Hz, the acoustic loss at this frequency is 20.43dB. We also show that by increasing the amplitude and the length of the undulation surface, the acoustic loss over the surface tends to also increase. This loss is estimated to be about 1.0dB for a change of about $1/2$ octave of frequency change from the optimal frequency.

The ground impedance rate is found to be important to the study of acoustic wave propagation. We observed that very soft surfaces (vegetation, grasses, etc.) with an impedance of 1 absorb two times more sound pressure compared to a hard surface (infinite impedance) and the

closer the source of the noise is to the ground, the more the sound pressure will be attenuated by the ground. This is important for propagation over a long distance. In addition, the undulating nature of the boundary surface also causes quite significant loss of the low-frequency compared to the hard undulating surfaces.

For future research, we note the following:

1. The effect of frequency on noise and the distortion that it will produce on a typical explosion waveform is not well understood. Different methods to include these effects such as those based on inverse Fourier Transforms or a purely time-domain formulation must be carefully considered.
2. The derivations shown indicate the effect of undulation along a radial point away from the main source. The undulations are therefore basically one-dimensional. The size of these mounds and their off-plane effects must be addressed.
3. A parametric analysis showing the effect of geometry, frequency content, and impact location should be studied. A neural network or a fuzzy inference engine can be used to summarize the data relationships and can be used to derive design guidelines.

BIBLIOGRAPHY

1. K. Attenborough "Sound Propagation Close To the Ground," *34:51–82 Annual Rev. Fluid Mech. (2002).*
2. W. E. Baker, "Explosion in Air," *Wilfred Baker Engineering, San Antonio, TX, 1983*.
3. M. Y. H. Bangash, "Impact and Explosion: Analysis and Design," *CRC Press, Boca Raton, FL, 1993*.
4. H. Brick and M. Ochmann, "A half-space BEM for the simulation of sound propagation above an impedance plane," *J. Acoust. Soc. Am. (2008).*
5. L. Bouchet, T. Loyau, N. Hamzaoui and C. Boisson, "Calculation of acoustic radiation using equivalent-sphere methods," *J. Acoust. Soc. Am. 107, 2387-2397 (2000).*
6. C-X. Bi, X-Z. Chen and J. Chen, "Sound field separation technique based on equivalent source method and its application in nearfield acoustic holography," *J. Acoust. Soc. Am. 123, 1472-1478 (2008).*
7. J. S. Bradley and J. A. Birta, "On the sound insulation of wood stud exterior walls," *J. Acoust. Soc. Am. 110, 3086-3096 (2001).*
8. G. A. Deschamps, "Gaussian beam as a bundle of complex rays," *Electron. Lett. 7, 684–685 (1971).*
9. Delany, M. E and Bazley, E. N, "Acoustical properties of fibrous absorbent material," *Applied acoustics, 3: 105-116 (1970).*
10. T. F. W. Embleton, J. E. Piercy, and G. A. Daigle, "Effective ow resistivity of ground surfaces determined by acoustical measurements," *J. Acoust. Soc. Am. 43.50.Vt, 43.20.Hq, 43.28.Fp, 43.85.Bh (1983).*

11. T. F. W. Embleton, T. Isei, and J. E. Piercy, “Noise reduction by barriers on finite impedance ground," *J. Acoust. Soc. Am. 67, 46-58, (1980).*

12. J. A. Fawcett, "A scattering-chamber approach for solving finite rough surface scattering problems," *J. Acoust. Soc. Am. 118, 1348–1357 (2005).*

13. J. A. Fawcett, “Complex-image approximations to the half-space acousto-elastic Green’s function,” *J. Acoust. Soc. Am. PACS numbers: 43.30.Dr, 43.20.El. (2000).*

14. R. D. Ford, D. J. Sounders, and G. Kerry, “The acoustic pressure waveform from small unconfined charges of plastic explosive,” *J. Acoust. Soc. Am. 94, 408-417 (1993).*

15. M. Hornikx and J. Forssen, "The 2.5-dimensional equivalent sources method for directly exposed and shielded urban canyons," *J. Acoust. Soc. Am. 122, 2532-2541 (2007).*

16. R. Jeans and I. C. Mathews, "The wave superposition method as a robust technique for computing acoustic fields," *J. Acoust. Soc. Am. 92, 1156-1166 (1992).*

17. M. E. Johnson, S. J. Elliott, K-H. Baek, and J. Garcia-Bonito, "An equivalent source technique for calculating the sound field inside an enclosure containing scattering objects," *J. Acoust. Soc. Am. 104, 1221-1231 (1998).*

18. S-M. Kim and Y-H. Kim, “Structural-acoustic coupling in a partially opened plate-cavity system: Experimental observation by using nearfield acoustic holography,” *J. Acoust. Soc. Am. 109, 65-74 (2001).*

19. Y. Kluizenaar et al., "Urban road traffic noise and annoyance: The effect of a quiet facade," *J. Acoust. Soc. Am., 130, 1936-1942 (2011).*

20. G. H. Koopmann, L. Song and J. B. Fahnline, "A method for computing acoustic fields based on the principle of wave superposition," *J. Acoust. Soc. Am. 86, 2433-2438 (1989).*

21. U. J. Kurze, “Noise reduction by barriers," *J. Acoust. Soc. Am. 55, 504-518 (1974).*

22. T. Kundu, S. Banerjee and K. V. Jata, "An experimental investigation of guided wave propagation in corrugated plates showing stop bands and pass bands," *J. Acoust. Soc. Am. 120, 1217-1226 (2006).*

23. W. L. Li, T.W. Wu, A.F. Seybert "A Half-Space Boundary Element Method for Acoustic Problems With a Reflecting Plane of Arbitrary Impedance," *Journal of Sound and Vibration (Impact Factor: 1.61). 03/1994; 171(2):173–184. (1994).*

24. Y. L. Li and Michael J. White. "Near-field computation for sound propagation above ground using complex image theory," *Acoustical Society of America. PACS numbers: 43.28.Fp, 43.20 (1996).*

25. R. H. Lyon, "Noise reduction of rectangular enclosures with one flexible wall," *J. Acoust. Soc. Am. 35, 1791–1797 (1963).*

26. Z. Mackawa, "Noise reduction by screens," *Appl. Acoust., vol. 1, 157-173 (1968).*

27. P. A. Nelson and S. H. Yoon, "Estimation of acoustic source strength by inverse methods: part I, conditioning of the inverse problem," *Journal of Sound and Vibration, vol. 233, issue 4, 639-664 (2000).*

28. P. A. Nelson and S. H. Yoon, "Estimation of acoustic source strength by inverse methods: part II, experimental investigation of methods for choosing regularization parameters," *Journal of Sound and Vibration, vol. 233, issue 4, 665-701 (2000).*

29. P. M. Morse, "Transmission of sound through a circular membrane in a plane wall," *J. Acoust. Soc. Am. 40, 354–366 (1966).*

30. M. Ochmann. "The Source Simulation Technique for Acoustic Radiation Problems," *Acta Acustica united with Acustica - S. Hirzel Verlag , pp. 512-527(16), (1995).*

31. M. Ochmann, "The complex equivalent source method for sound propagation over an

impedance plane," *J. Acoust. Soc. Am. 116, 3304-3311 (2004).*

32. A. I. Papadopoulos, and C. G. Don, “A study of barrier attenuation by using acoustic impulses," *J. Acoust. Soc. Am. 90, 1011-1018 (1991).*
33. M. E. V. Pinho and J. R. Arrudo, "On the use of the equivalent source method for nearfield acoustic holography," *ABCM Symposium Series in Mechatronics, vol. 1, 590-599 (2004).*
34. C. Potel et al., "Lamb wave attenuation in a rough plate. II. Analytical and numerical results in a fluid plate," *Journal of Applied Physics, vol. 104, 2008.*
35. L. Raleigh, *The Theory of Sound.* Macmillan and Co., London", vol. 2, 1929.
36. W. Reed, "Atmospheric attenuation of explosion waves," *J. Acoust. Soc. Am. 61, 39-47 (1977).*
37. D. J. Saunders and R. D. Ford, “A study of the reduction of explosive impulses by finite sized barriers,” *J. Acoust. Soc. Am. 94, 2859–2875 (1993).*
38. P. D. Schomer, E. Buchta and K-W. Hirch, “Decibel annoyance reduction of low-frequency blast attenuating windows,” *J. Acoust. Soc. Am. 89, 1708-1713 (1991).*
39. P. Schomer and A. Averbuch, “Indoor human response to blast sounds that generates rattles,” *J. Acoust. Soc. Am. 82, 665-673 (1989).*
40. L. Song, G. H. Koopman, and J. Fahnline, “Numerical errors associated with the method of superposition for computing acoustic fields,” *J. Acoust. Soc. Am. 89, 2625–2633 (1991).*
41. M. Vang and M. Bikdash, "Simulation Study of Low-Frequency Outdoor Noise Reduction Using Undulating Landscaping," *IEEE SoutheastCon 2009, 416-421 (2009).*
42. M Vang and Marwan Bikdash “Modeling the effect of hard undulating surface on outdoor

noise using equivalent sources," *IEEE Southeast Con 2009, 183 - 187 (2011).*

43. F. Walkden and M. West, "Prediction of enhancement factor for small explosive sources in a stratified moving atmosphere," *J. Acoust. Soc. Am. 84, 321-326 (1988).*
44. Z. Wang and S. F. Wu, "Helmholtz equation-least-squares method for reconstructing the acoustic pressure field," *J. Acoust. Soc. Am. 102, 2020–2032 (1997).*
45. S. F. Wu and J. Yu, "Reconstructing interior acoustic pressure fields via Helmholtz equation least-squares method," *J. Acoust. Soc. Am. 104, 2054–2060 (1998).*